Expedition 358 Preliminary Report

NanTroSEIZE Plate Boundary Deep Riser 4: Nankai Seismogenic/Slow Slip Megathrust

7 October 2018-31 March 2019

Harold Tobin, Takehiro Hirose, Matt Ikari, Kyuichi Kanagawa, Gaku Kimura, Masataka Kinoshita, Hiroko Kitajima, Demian Saffer, Asuka Yamaguchi, Nobuhisa Eguchi, Lena Maeda, Sean Toczko, and the Expedition 358 Scientists



Publisher's notes

Core samples and the wider set of data from the science program covered in this report are under moratorium and accessible only to Science Party members until 18 July 2020.

This publication was prepared by the D/V *Chikyu* Science Operator, the Institute for Marine-Earth Exploration and Engineering (MarE3), at the Japan Agency for Marine-Earth Science and Technology (JAMSTEC) and the *JOIDES Resolution* Science Operator (JRSO) at Texas A&M University (TAMU) as an account of work performed under the International Ocean Discovery Program (IODP). Funding for IODP is provided by the following international partners:

National Science Foundation (NSF), United States Ministry of Education, Culture, Sports, Science and Technology (MEXT), Japan European Consortium for Ocean Research Drilling (ECORD)

Portions of this work may have been published in whole or in part in other IODP documents or publications.

Disclaimer

Any opinions, findings, and conclusions or recommendations expressed in this publication are those of the author(s) and do not necessarily reflect the views of the participating agencies, TAMU, or Texas A&M Research Foundation.

Copyright

Except where otherwise noted, this work is licensed under the Creative Commons Attribution 4.0 International (CC BY 4.0) license (https://creativecommons.org/licenses/by/4.0/). Unrestricted use, distribution, and reproduction are permitted, provided the original author and source are credited.



Citation

Tobin, H., Hirose, T., Ikari, M., Kanagawa, K., Kimura, G., Kinoshita, M., Kitajima, H., Saffer, D., Yamaguchi, A. Eguchi, N., Maeda, L., Toczko, S., and the Expedition 358 Scientists, 2019. *Expedition 358 Preliminary Report: Nan-TroSEIZE Plate Boundary Deep Riser 4: Nankai Seismogenic/Slow Slip Megathrust.* International Ocean Discovery Program. https://doi.org/10.14379/iodp.pr.358.2019

ISSN

World Wide Web: 2372-9562

Expedition 358 participants

Expedition 358 scientists

Harold Tobin

Science Leader/Co-Chief Scientist

Department of Earth and Space Sciences

University of Washington

USA

htobin@uw.edu

Takehiro Hirose

Science Leader/Co-Chief Scientist

Kochi Institute for Core Sample Research

Japan Agency for Marine-Earth Science and Technology Japan

hiroset@jamstec.go.jp

Matt Ikari

Science Leader/Co-Chief Scientist

Center for Marine Environmental Sciences (MARUM)

University of Bremen

Germany

mikari@marum.de

Kyuichi Kanagawa

Science Leader/Co-Chief Scientist

Department of Earth Sciences

Graduate School of Science/Faculty of Science

Chiba University

Japan

kyu_kanagawa@faculty.chiba-u.jp

Gaku Kimura

Science Leader/Co-Chief Scientist

Tokyo University of Marine Science and Technology

Japan

gkimur0@kaiyodai.ac.jp

Masataka Kinoshita

Science Leader/Co-Chief Scientist

Earthquake Research Institute

University of Tokyo

Japan

masa@eri.u-tokyo.ac.jp

Hiroko Kitajima

Science Leader/Co-Chief Scientist

Department of Geology and Geophysics

Texas A&M University

USA

kitaji@tamu.edu

Demian Saffer

Science Leader/Co-Chief Scientist

Department of Geosciences

The Pennsylvania State University

USA

dms45@psu.edu

Asuka Yamaguchi

Science Leader/Co-Chief Scientist

Atmosphere and Ocean Research Institute

University of Tokyo

Japan

asuka@aori.u-tokyo.ac.jp

Nobuhisa Eguchi

Expedition Project Manager

Institute for Marine-Earth Exploration and Engineering Japan Agency for Marine-Earth Science and Technology Japan

neguchi@jamstec.go.jp

Lena Maeda

Expedition Project Manager

Institute for Marine-Earth Exploration and Engineering Japan Agency for Marine-Earth Science and Technology Japan

maedal@jamstec.go.jp

Sean Toczko

Lead Expedition Project Manager

Institute for Marine-Earth Exploration and Engineering Japan Agency for Marine-Earth Science and Technology Japan

sean@jamstec.go.jp

John Bedford

Physical Properties Specialist

Department of Earth, Ocean and Ecological Sciences

University of Liverpool

Jane Herdman Laboratories

United Kingdom

jbedford@liverpool.ac.uk

Shun Chiyonobu

Paleontologist Specialist

Faculty of International Resource Sciences

Akita University

Japan

chiyo@gipc.akita-u.ac.jp

Tobias August Colson

Real-Time Geomechanics

Santos Ltd.

Australia

tobias.colson@santos.com

Marianne Conin

Logging Specialist

Georesources

Campus ARTEM

Ecole des Mines de Nancy

University of Lorraine

France

marianne.conin@univ-lorraine.fr

Pauline H. Cornard Sedimentologist

Earth Sciences Department University College London United Kingdom pauline.cornard.15@ucl.ac.uk

Armin Dielforder

Structural Geologist/Sedimentologist

Helmholtz Centre Potsdam GFZ German Research Centre for Geosciences Germany armin.dielforder@gfz-potsdam.de

Mai-Linh Doan

Logging Specialist/Physical Properties Specialist

Laboratoire ISTerre Université Grenoble-Alpes France

mai-linh.doan@univ-grenoble-alpes.fr

Jade Dutilleul

Structural Geologist

Georesources

Ecole Nationale Supérieure de Géologie

University of Lorraine

France

jade.dutilleul@univ-lorraine.fr

Daniel Roy Faulkner

Structural Geologist

Department of Earth, Ocean and Ecological Sciences University of Liverpool

United Kingdom

Faulkner@liv.ac.uk

Rina Fukuchi

Sedimentologist

Department of Ocean Floor Geoscience Atmosphere and Ocean Research Institute University of Tokyo

rfukuchi@aori.u-tokyo.ac.jp

Gilles Guérin

Logging Specialist

Borehole Research Group Lamont-Doherty Earth Observatory Columbia University **USA**

guerin@ldeo.columbia.edu

Yohei Hamada

Logging Specialist

Kochi Institute for Core Sample Research Japan Agency for Marine-Earth Science and Technology Japan

yhamada@jamstec.go.jp

Mari Hamahashi Sedimentologist

Earth Observatory of Singapore Nanyang Technological University Singapore

mhamahashi@ntu.edu.sg

Wei-Li Hong

Mud Gas Specialist

Geological Survey of Norway Norway

wei-li.hong@ngu.no

Akira Ijiri

Geochemist/Mud Gas Specialist

Kochi Institute for Core Sample Research Japan Agency for Marine-Earth Science and Technology Japan

ijiri@jamstec.go.jp

Dominik Jaeger Sedimentologist

Department of Geology University of Innsbruck Austria

dominik.jaeger@uibk.ac.at

Tamara Jeppson **Logging Specialist**

Department of Geology and Geophysics Texas A&M University USA

tjeppson@tamu.edu

Zirou Jin

Physical Properties Specialist

Geological Engineering University of Wisconsin-Madison USA zjin62@wisc.edu

Barbara E. John **Structural Geologist**

Department of Geology and Geophysics University of Wyoming **USA**

bjohn@uwyo.edu

Manami Kitamura

Physical Properties Specialist

Research Institute for Geo-Resources and Environment Geological Survey of Japan National Institute of Advanced Industrial Science and Technology Japan

kitamura.m@aist.go.jp

Achim Kopf

Mud Gas Specialist

Center for Marine Environmental Sciences (MARUM)

University of Bremen

Germany

akopf@marum.de

Harue Masuda

Geochemist/Mud Gas Specialist

Department of Biology and Geosciences

Osaka City University

Japan

harue@sci.osaka-cu.ac.jp

Atsushi Matsuoka

Paleontologist

Department of Geology

Niigata University

Japan

amatsuoka@geo.sc.niigata-u.ac.jp

Gregory F. Moore

Logging Specialist

Department of Earth Sciences

University of Hawaii at Manoa

Hawaii

USA

gmoore@hawaii.edu

Makoto Otsubo

Structural Geologist

Research Institute of Earthquake and Volcano Geology

Geological Survey of Japan

National Institute of Advanced Industrial Science and

Technology

Japan

otsubo-m@aist.go.jp

Christine Regalla

Structural Geologist

Department of Earth and Environment

Boston University

USA

Present affiliation (9 October 2019):

School of Earth and Sustainability

Northern Arizona University

USA

christine.regalla@nau.edu

Arito Sakaguchi

Sedimentologist

Graduate School of Sciences and Technology for Innovation

Yamaguchi University

Japan

arito@yamaguchi-u.ac.jp

James Sample

Sedimentologist/Geochemist

School of Earth and Sustainability

Northern Arizona University

USA

james.sample@nau.edu

Anja Schleicher

Sedimentologist

Helmholtz Centre Potsdam

GFZ German Research Centre for Geosciences

Germany

anja.schleicher@gfz-potsdam.de

Hiroki Sone

Physical Properties Specialist

Geological Engineering

University of Wisconsin-Madison

USA

hsone@wisc.edu

Katja Stanislowski

Physical Properties Specialist

Center for Marine Environmental Sciences (MARUM)

University of Bremen

Germany

kstanislowski@marum.de

Michael Strasser

Sedimentologist

Department of Geology

University of Innsbruck

Austria

michael.strasser@uibk.ac.at

Tomohiro Toki

Geochemist/Mud Gas Specialist

University of the Ryukyus

Japan

toki@sci.u-ryukyu.ac.jp

Takeshi Tsuji

Logging Specialist

Department of Earth Resources Engineering

Kyushu University

Japan

tsuji@mine.kyushu-u.ac.jp

Kohtaro Ujiie

Structural Geologist

Graduate School of Life and Environmental Sciences

University of Tsukuba

Japan

kujiie@geol.tsukuba.ac.jp

Michael Underwood

Sedimentologist

Department of Earth and Environmental Science New Mexico Institute of Mining and Technology

USA

underwoodm@missouri.edu

Suguru Yabe

Logging Scientist

Research Institute of Earthquake and Volcano Geology

Geological Survey of Japan

National Institute of Advanced Industrial Science and

Technology

Japan

s.yabe@aist.go.jp

Yuzuru Yamamoto

Structural Geologist

Center for Mathematical Science and Advanced Technology Japan Agency for Marine-Earth Science and Technology Japan

yuzuru-y@jamstec.go.jp

Junli Zhang

Mud Gas Specialist

Center for Marine Environmental Sciences (MARUM)

University of Bremen

Germany

jzhang@marum.de

Yohei Hamada

Logging Staff Scientist

Kochi Institute for Core Sample Research Japan Agency for Marine-Earth Science and Technology

yhamada@jamstec.go.jp

Yoshinori Sanada

Logging Staff Scientist

Institute for Marine-Earth Exploration and Engineering Japan Agency for Marine-Earth Science and Technology Japan

sanada@jamstec.go.jp

Videographers

Dan Brinkhuis

Videographer

The Netherlands

dan@sciencemedia.nl

NanTroSEIZE chief project scientists

Masataka Kinoshita

Chief Project Scientist

Earthquake Research Institute

University of Tokyo

Japan

masa@eri.u-tokyo.ac.jp

NanTroSEIZE science coordinators

Kyuichi Kanagawa

Structural Geology

Department of Earth Sciences

Graduate School of Science/Faculty of Science

Chiba University

Japan

kyu_kanagawa@faculty.chiba-u.jp

Gaku Kimura

Structural Geology

Tokyo University of Marine Science and Technology

gkimur0@kaiyodai.ac.jp

Yukari Kido

Logging Staff Scientist

Institute for Marine-Earth Exploration and Engineering Japan Agency for Marine-Earth Science and Technology Japan

ykido@jamstec.go.jp

Erwan Le Ber

Logging Staff Scientist

University of Leicester United Kingdom

elb51@leicester.ac.uk

Saneatsu Saito

Logging Staff Scientist

Research and Development Center for Ocean Drilling Science Japan Agency for Marine-Earth Science and Technology Japan

saito@jamstec.go.jp

Dick Peterse Videographer

The Netherlands

dick@sciencemedia.n

Harold Tobin

Chief Project Scientist

Department of Earth and Space Sciences

University of Washington

USA

htobin@uw.edu

Achim Kopf

Geochemistry

Center for Marine Environmental Sciences (MARUM)

University of Bremen

Germany

akopf@marum.de

Gregory F. Moore

Geophysics

Department of Earth Sciences University of Hawaii at Manoa

Hawaii

USA

gmoore@hawaii.edu

Demian Saffer

Geomechanics and Physical Properties

Department of Geosciences The Pennsylvania State University USA

dms45@psu.edu

Michael Strasser Stratigraphy

Department of Geology University of Innsbruck Austria

michael.strasser@uibk.ac.at

Operational and technical staff

Shipboard personnel and technical representatives

Captains (Mantle Quest Japan)

Yukio Dowaki Takemasa Kobayashi

Offshore Installation Manager (Mantle Quest Japan)

Masayuki Kawasaki

Tool Pushers/Coring Supervisors (Mantle Quest Japan)

Teruyuki Koyama Charles Ronald Paul MacGregor Paul Thornton

Underreamer Engineer (NOV)

Glyn Christopher Edwards

Operations Superintendents (MarE3)

Terumichi Ikawa Tomokazu Saruhashi

Drilling Engineers (MarE3)

Kaz Nishiyama Noriaki Sakurai Tao Shiotani Akio Suzuki Takahiko Yokoyama

Real-Time Geomechanics

Kan Aoike Emily Wisbey Adam Wspanialy

Downhole Tools Engineers (Halliburton)

Laurynas Cernauskas Wedcharat Chuaybudda Gustavo Zarif Camacho Davila Monpanu Galjaru Joseph Brett Lyman Alex Munro Feng Pang Adrianus Andi Prijatno Cedric Vanya Lutonda

Michael B. Underwood Lithostratigraphy

Department of Earth and Environmental Science New Mexico Institute of Mining and Technology USA

underwoodm@missouri.edu

Yasu Yamada Downhole Logging

Research and Development Center for Ocean Drilling Science Japan Agency for Marine-Earth Science and Technology Japan

yyamada@jamstec.go.jp

Directional Drilling Engineers (Halliburton)

Bob Manjenic Gavin Meikle Daniel Justin Priestly

Mud Logging Engineers (Geoservices)

Aung Kaw Myint (Data Engineer)
Pravin Maruti Patil (Data Engineer)
Ya Wai (Data Engineer)
Myint Win (Data Engineer)
Aung Kaung (Mud Logger)
Zin Maung Maung Lwin (Mud Logger)
Rawikan Mojarin (Mud Logger)
Phyoe Wai (Mud Logger)
Tania Uli Crocker (Sample Catcher)

Mohamed Idris Bin Hohamed Ismail (Sample Catcher)

Nurul Najihah (Sample Catcher) Samantha Usun (Sample Catcher)

Mud Engineers (Telnite)

Ryohei Yaya Hiroki Ishikawa Katsuki Mori Masato Sawaguchi

Wireline Tool Engineers (Schlumberger)

Gan Lifeng Kengo Tsuchida Yusuke Yoshii Akira Yoshizawa

Laboratory Officer (Marine Works Japan)

Tomoyuki Tanaka

Assistant Lab Officers (Marine Works Japan)

Toru Fujiki Soichi Moriya Toshikuni Yabuki

Curators (Marine Works Japan)

Shigako Nigi Masaru Yasunaga

Laboratory Technicians (Marine Works Japan)

Masayuki Abe Nobuhiro Anraku Akihiko Fujihara Keiko Fujino Kei Fujiya

Mikio Hasegawa Kentaro Hatakeda Ei Hatakeyama Yuya Hitomi Daiki Kawata Yoshiki Kido Susumu Konno

Reina Miyahara Hirotaka Miyamoto

Koh Morita Htet Naing Lin Saori Nishino Rui Nitahara Yuta Oda Yasusei Sato Ritsuko Sawada Yu Shimazaki Yuta Shinomiya Kazuma Takahashi

Hiromi Takeda

Tomonori Watai

Mika Yamaguchi Hideki Yamamoto Masahiro Yasuda Kanako Yoshida Paing Zu

Operation Geologists (MarE3)

Kan Aoike

Takamitsu Sugihara Kentaro Takeda Ryuta Tanaka

Assistant Operation Geologists (Marin Works Japan)

Atushi Kurasawa Masumi Sakaguchi

Technical Engineers (MarE3)

Junya Ishiwata Yasuhiro Namba Ryuta Tanaka

Coring Specialist (MarE3)

Yuichi Shinmoto

Publications Specialists (Marine Works Japan)

Akiko Fuse Mika Saido

Abstract

International Ocean Discovery Program (IODP) Expedition 358 was carried out from October 2018 through March 2019 on the D/V Chikyu in an attempt to reach a plate boundary fault zone at seismogenic depths for the first time in scientific ocean drilling. The goal was to extend Hole C0002P from ~2900 to ~5200 meters below seafloor (mbsf) and cross the seismically interpreted main décollement fault zone with logging while drilling (LWD), downhole stress measurements, cuttings sampling, mud gas sampling, and partial coring by drilling a sidetrack to create a new hole (C0002Q). Although drilling reached 3262.5 mbsf, the deepest to date in all of scientific ocean drilling, the effort to drill to and sample the target-the megathrust fault zone-was not successful. Operational challenges in establishing sidetrack holes and advancing them at reasonable rates of penetration limited the new cased hole interval to less than 60 m total at a depth shallower than the previously established casing depth of 2922 mbsf. Combined, the cuttings, logs, and ~60 cm of recovered core from sidetrack Holes C0002Q-C0002T revealed hemipelagic sediments and fine silty turbidites consistent in lithology and physical properties with those recovered in the same depth interval at the same site during Integrated Ocean Drilling Program Expedition 348. Cuttings revealed evidence of only weakly deformed rock, with relatively common calcite veins but few other structural indicators. Because no downhole leak-off tests were made and very little borehole imaging was performed, no further insight into the tectonic context was acquired.

After riser drilling at Site C0002 was terminated, drilling at alternate contingency Sites C0024 and C0025 was carried out. Site C0024 targeted the frontal thrust region to sample and log hanging wall rocks and the shallow portion of the décollement zone, and Site C0025 accessed sediments in the Kumano fore-arc basin. At Site C0024, a dedicated logging hole was drilled and a very complete suite of logs were acquired from 0 to 869 mbsf. Preliminary interpretation of log response and images suggests the frontal thrust zone was encountered from about 813 mbsf to the base of the hole, with a zone of notably low resistivity and steep bedding from 850 mbsf to the bottom of the hole. Core samples revealed lithologic units interpreted to be hemipelagic and turbiditic basin fill, trench fill, and Shikoku Basin sediments and encountered deformation potentially associated with a back thrust imaged in seismic reflection data. However, coring had to be terminated at about 620 mbsf, well short of the frontal thrust zone. Site C0025 recovered fore-arc basin sediments underlain by those interpreted to have been deposited in a trench-slope basin setting; no clear transition into older, inner accretionary wedge material was identified during preliminary analysis. Coring from 400 to 571 mbsf yielded datable material and possible evidence for diapiric intrusion of sediments.

Introduction and background

The Nankai Trough Seismogenic Zone Experiment (NanTro-SEIZE) program is a coordinated, multiexpedition drilling project designed to investigate fault mechanics and seismogenesis along the Nankai subduction megathrust (Figure F1) through direct sampling, in situ measurements, and long-term monitoring in conjunction with allied laboratory and numerical modeling studies (Tobin and Kinoshita, 2006; Tobin et al., 2015a, 2019). The fundamental scientific objectives of the NanTroSEIZE project include characterizing the nature of fault slip and strain accumulation, fault and wall rock composition, fault architecture, and state variables throughout

the active plate boundary system. Eleven previous expeditions have been carried out, establishing a transect of sites from the incoming (subducting) plate through fault zone and accretionary wedge characterization and into the central fore-arc basin (Figure F2). For reviews of many of the principal results from these sites, see Underwood and Moore (2012), Ujiie and Kimura (2014), and Tobin et al. (2015b, 2019).

Site C0002 is located in the Kumano fore-arc basin above the seismogenic, partially locked portion of the plate boundary thrust system (Figures F1, F2, F3). The Kumano Basin sedimentary sequence and uppermost part of the accretionary prism were drilled, logged, and sampled during Integrated Ocean Drilling Program Expeditions 314 (logging while drilling [LWD] to 1401.5 meters below seafloor [mbsf]), 315 (coring to 1057 mbsf), 338 (LWD to 2005 mbsf and coring to 1120 mbsf), and 348 (LWD to 3058.5 mbsf, with limited coring from 2163 to 2218.5 mbsf) (Expedition 314 Scientists, 2009; Expedition 315 Scientists, 2009; Strasser et al., 2014; Tobin et al., 2015b).

The principal goal of International Ocean Discovery Program (IODP) Expedition 358 was to reach and sample the reflector identified as the likely plate boundary fault at Site C0002 by extending the riser borehole (Hole C0002P) established during previous Integrated Ocean Drilling Program NanTroSEIZE expeditions (Figure **F3**). This drilling target is also in close proximity to the location of very low frequency (VLF) earthquakes and the first tectonic tremor recorded in any accretionary prism setting (summarized in Obara and Kato, 2016), all of which suggest fault processes related to the updip limit of megathrust seismogenic mechanics are active here. Recent results from the NanTroSEIZE long-term borehole monitoring systems and Dense Oceanfloor Network System for Earthquakes and Tsunamis (DONET) seafloor observations further suggest that the plate boundary at this location is partially locked and partially releasing plate convergence strain in these slow slip events accompanied by low-frequency tectonic tremor and VLF earthquakes (Araki et al., 2017).

A detailed drilling plan was developed by the Center for Deep Earth Exploration (CDEX) after careful analysis of the Expedition 338 and 348 drilling experiences (Figure F4). It involved sidetracking from near the bottom of the Hole C0002P casing pipe at 2880 mbsf to begin Hole C0002Q and then advancing in three casing stages, alternately drilling and then cementing in successive casing strings to reach the zone just ~200 m above the anticipated plate boundary fault zone. A comprehensive suite of LWD measurements were planned, along with detailed cuttings analysis, to monitor progress and characterize the lower accretionary wedge/hanging wall of the fault zone. The final stage of operations was planned to drill across the high-amplitude seismic reflector identified as the main plate boundary fault zone with LWD and then drill an open hole sidetrack for a second pass to core 100–200 m in total from the hanging wall across the fault and into the footwall (Figure F4).

For the ~2000 m interval of planned drilling above the target zone, the primary scientific objectives were to (1) determine the composition, stratigraphy, and deformational history of the Miocene accretionary wedge; (2) reconstruct its thermal, diagenetic, and metamorphic history; (3) determine horizontal stress orientations and magnitudes; and (4) investigate the mechanical and hydrological properties of the upper plate of the seismogenic plate boundary. In the target zone, a comprehensive structural, lithologic/petrologic, and physical properties characterization of the fault zone and wall rocks was planned using cuttings, logging, and continuous core sampling. The final objective was to leave the bore-

hole in a condition that would allow for the design and deployment of a long-term in situ borehole observatory system subsequent to the expedition.

Previous major riser drilling efforts during Expeditions 338 and 348 advanced the main riser hole at Site C0002 (Hole C0002F/C0002N/C0002P) to 3058.5 mbsf, and casing was installed in that hole to 2922.5 mbsf (Figures F3, F4A). Extensive downhole logging data, continuously sampled drill cuttings, and limited intervals of core were collected during those expeditions.

Principal results

Site C0002

Summary of planned Site C0002 riser operations for Expedition 358:

- Employing the riser drilling technique, kick off from at or above the existing 11¾ inch casing shoe at 2922.5 mbsf and open a new hole to ~5200 mbsf or the maximum achievable depth within time and budget limits, setting 9½ inch (expanded to 11¾ inch) casing, 9¾ inch steel liner, and 7½ inch (expanded to 9¾ inch) casing to ~4700 mbsf and open hole drilling with an 8½ inch diameter bit below that to total depth (TD).
- Use a suite of LWD/measurement-while-drilling tools and measurements to include gamma ray, sonic, and resistivity logs and images. Sample and analyze lithology, physical properties, and geochemistry of cuttings from the entire drilled interval at a suitable spacing (nominally every 5 m).
- At casing set points and other opportunities, conduct downhole tests—formation integrity test (FIT), extended leak-off tests (XLOTs), leak-off tests (LOTs), and other formation tests—to evaluate the in situ stress, pore fluid pressure, permeability, and rock strength conditions.
- Core about 100 m: ~50 m from 4650 mbsf and ~50 m from 5150 mbsf or at a depth selected as we penetrate the fault zone.

During the expedition, extensive difficulties establishing the sidetracks and advancing the boreholes plagued the operation from the outset and continuously as a series of mitigation strategies were attempted (Figures F4C, F5). A more complete history of the operations appears below. In summary, riser drilling in Hole C0002Q advanced only to 3262.5 mbsf (204 m deeper than Hole C0002P) before it had to be abandoned. Cuttings were obtained from this hole, but only a very basic LWD data set was acquired, including gamma ray and a resistivity log, rather than the full planned suite that was to include resistivity imaging logs and sonic and check shot seismic data. A second sidetrack was established at 2790 mbsf, and Hole C0002R advanced to 3085 mbsf (Figure F5), again with only cuttings and basic logs acquired. Hole C0002S was sidetracked and met a fate similar to that of Hole C0002R, ending at 2933 mbsf. The final sidetrack Hole C0002T was made, and three cores with minimal recovery were collected from 2836.5 to 2848.5 mbsf before riser operations came to an end.

Unfortunately, these technical setbacks resulted in only very modest scientific achievements at Site C0002. New cores were obtained ~600 m deeper than any previous cores from Expedition 348 and before. Cuttings and limited logs were obtained from ~204 m of new drilling depth but came 2000 m short of the target. No downhole measurements related to in situ stress conditions were obtained.

Scientific results from cuttings, logs, mud gas monitoring, and cores of sidetrack Holes C0002Q–C0002T are reported in this section (Figure **F6**).

Lithology

We analyzed cuttings from four overlapping holes (Holes C0002Q-C0002T) and three cores from Hole C0002T. The combined depth interval for those samples extends from 2812.5 to 3257.5 mbsf. We found four rock types with gradational lithologic attributes. Fine silty claystone is light gray to gray in color. Its poorly consolidated cuttings are typically rounded and sticky. Silty claystone is gray to olive black and more lithified, and its cuttings are angular and fissile. Siltstone shows a higher degree of consolidation, and its cuttings are angular. There are two varieties of sandstone: (1) gray, very fine grained, and angular and (2) light gray, fine grained, less consolidated, and more rounded. Silty claystone is the dominant lithology in Holes C0002Q-C0002T, composing 35%-80% of the total cuttings (Figure F6). All other lithologies are subordinate, and fine silty claystone decreases to minor amounts. Collectively, all sedimentary rocks correlate with Lithologic Unit V as defined during Expedition 348 (Tobin et al., 2015b).

X-ray diffraction (XRD) shows that clay minerals (smectite + illite + chlorite + kaolinite) are the most abundant mineral constituent, with normalized percentages of ~40-55 wt% (Figure F6). Proportions change somewhat with grain size; values for quartz and feldspar are about 5-10 wt% larger in handpicked sandstone and siltstone samples, and abundances of total clay minerals in coarser lithologies are smaller by about 10-20 wt%. Calcite is usually below the detection limit by XRD (<1 wt%). When compared to bulk cuttings at corresponding depths from Hole C0002P, we notice a systematic shift toward modestly higher proportions of quartz and feldspar. Those variations in bulk mineralogy are probably a reflection of natural heterogeneity in a steeply dipping succession of interbedded silty claystone, siltstone, and fine sandstone. Overall, X-ray fluorescence (XRF) results exhibit no significant depth-dependent trends in bulk sediment geochemistry except for a slight increase in MgO with depth. The chemical uniformity within and among the individual holes is consistent with relatively homogeneous proportions of rock types.

The depth interval assigned to Lithologic Subunit VB in Hole C0002P is characterized by abundant fine silty claystone and rare sandstone (Tobin et al., 2015b). The facies was interpreted to be a hemipelagic depositional environment punctuated by sporadic finegrained turbidity currents (Tobin et al., 2015b). The same depth interval in Holes C0002Q–C0002T appears to contain more fine sandstone and siltstone. These deposits are likewise consistent with mostly hemipelagic deposition but contain modestly higher occurrences of silt and fine-sand turbidity currents. The environment of deposition is therefore likely to have been a trench or an abyssal plain seaward of the trench.

Structural geology

Very few identified deformation-related features (<1% of total cuttings exhibit them) occur between 2827.5 and 3257.5 mbsf. Granular and dogtooth calcite veins occur throughout the interval; slickenlines and stepped striae are rare. No scaly fabrics, minor faults, or cataclastic bands were recovered in cuttings from Holes C0002Q–C0002T. The low abundance of deformation structures suggests that the sections of Holes C0002Q–C0002T between 2827.5 and 3262.5 mbsf are weakly deformed.

Mineral veins record different modes and phases of vein formation; crack-seal veins document repeated episodes of extensional fracturing potentially driven by fluctuations in pore fluid pressure or prevailing stress state. Extensional fracturing can be followed by shear deformation as recorded by shear veins and/or slickenlines partially overprinting crack-seal veins and vice versa.

Geochemistry

At Site C0002, mud gas was analyzed from Holes C0002Q-C0002T and compared to earlier drilling in Hole C0002P during Expedition 348 (Tobin et al., 2015b). In addition, cuttings and cores were analyzed for headspace gas content and CaCO₃, total organic carbon, and total nitrogen. Mud gas composition reveals trends similar to the shallower riser drilling during Expedition 348, with decreasing CH₄ and C₁/C₂ ratios downhole, whereas the δ¹³C-CH₄ values remain largely between about -50% and about -40%, characteristic of thermogenic gas. Spikes toward higher methane concentrations seen at ~2950, ~3050, and ~3200 mbsf are accompanied by elevated H₂ and ²²²Rn in the mud gas. In contrast, no such elevated concentrations were found in these depth intervals when analyzing the cuttings. All hydrocarbons as well as CO decrease with depth, and n-butane and H2 are particularly low from ~3050 mbsf downhole. We suspect that the spikes in real-time mud gas monitoring reflect fluid migration in minor fault zones that would likely not be evident when analyzing cuttings.

Biostratigraphy and paleomagnetism

Preliminary age determination for cuttings from Holes C0002Q-C0002T is based exclusively on the examination of calcareous nannofossils. The abundance and preservation of calcareous nannofossils varies throughout the sequence. Different states of abundance and preservation are recognized even in different pieces from the same cuttings sample. Nannofossil assemblages from the four holes all contain Reticulofenestra pseudoumbilicus with a diameter greater than or equal to 7 µm, except for a single piece from Slide C of Sample 358-C0002Q-365-SMW (3027.5 mbsf). R. pseudoumbilicus (≥7 μm) has an age range of 12.8-3.63 Ma with an interval of absence between 8.8 and 7.09 Ma. Assemblages recovered from 2917.5 to 3257.5 mbsf (Hole C0002Q), from 2817.5 to 3077.5 mbsf (Hole C0002R), and from 2847.5 to 2933.5 mbsf (Hole C0002S) can be assigned either to 12.8-8.8 or 7.09-3.63 Ma. An assemblage from Slide C of Sample 365-SMW (3027.5 mbsf) that lacks R. pseudoumbilicus $(\geq 7 \mu m)$ is indicative of an age between 8.8 and 7.09 Ma.

Radiolarians and foraminifers were also found in Holes C0002Q–C0002S but were not used for age determination because of very rare occurrences. All radiolarians are possibly of reworked origin.

Remanent magnetizations of archive-half sections from Hole C0002T were measured but did not yield useful results regarding magnetic polarity because of poor core quality and recovery.

Physical properties

In Holes C0002Q–C0002T, physical properties measurements were conducted mostly on cuttings samples augmented by a few core samples from Hole C0002T. Moisture and density (MAD) measurements show that porosity of handpicked intact cuttings decreases from about 19% at 2800 mbsf to about 17% at 3250 mbsf (Figure F6A), which is in good agreement with the trend found for Hole C0002P during Expedition 348. The porosity for bulk cuttings from Hole C0002Q was 10%–20% higher than that of intact cuttings at depths overlapping Hole C0002P, which is again consistent with

results from Hole C0002P, but the difference became smaller, or nonexistent, toward the deeper section of Hole C0002Q and in the remaining Holes C0002R–C0002T. The thermal conductivity measured on a core sample from Hole C0002T follows the trend suggested from previous expeditions.

Logging

In Hole C0002Q (logging interval = 2888–3262 mbsf), phase resistivity remains almost uniform over most of the logged interval and ranges between 2 and 3 Ωm (Figure F6). Gamma ray is slightly more variable, suggesting a mostly uniform lithology, with short excursions to lower values that could indicate fine sandy intervals or other minor lithologies. These logging responses fit the characteristics of Logging Subunit Ve identified in the deeper section of Hole C0002P (Tobin et al., 2015b), suggesting that the entire logged interval belongs to the same subunit.

In Hole C0002Q at 2907–2916 mbsf, borehole failures are observed in a northwest–southeast orientation. The southeastern conductive zone has a larger width (\sim 93°) than the northwestern zone (\sim 61°). Because the southeast and northwest azimuths are approximately equivalent to the upper and lower sides of the deviated borehole, respectively, the wider low resistivity zone in the southeast orientation, or at the top of the hole, indicates that the tool was separated from the upper side of the borehole. In contrast, the narrower low resistivity zone on the northwest, or bottom, side of the hole indicates that the tool was largely in contact with the bottom side of the borehole. Therefore, the narrower low resistivity zone in the northwest is considered to reflect the actual width of the borehole failure. The average width of the northwest borehole failure is 61°, and the maximum value is 86°.

Site C0024

With 28 days remaining in the expedition after the termination of riser operations at Site C0002, drilling was conducted at two alternate contingency sites. Site C0024 is located a few kilometers landward (northwest) of IODP Site C0006 in the frontal anticline overlying the frontal thrust (Figure F7). It targeted the hanging wall geology and the main frontal thrust at ~820 mbsf. An LWD hole was drilled into and penetrated the frontal thrust, which is interpreted to be a complex zone of fault strands and imbrication of thrust slices. Coring was attempted in the zone below 500 mbsf, as well as in several shallower intervals, but had to be abandoned because of deteriorating borehole conditions before reaching the main fault zone as identified in log and seismic data. Results from all holes at Site C0024 are summarized in this section (Figure F8).

Lithology

The stratigraphic section at Site C0024 is divided into four lithologic units (Figure **F8A**). Lithologic Unit I is composed of silty clay to clayey silt. We set the base of Unit I at the top of the uppermost turbidite in Hole C0024B at 3.76 mbsf. No age-diagnostic nannofossils were identified in this interval, so the Holocene age is only inferred. The base of Unit I is a prominent unconformity.

Most of Lithologic Unit II is 1.59-1.67 Ma in age and composed of four lithologies in a continuum of gradational attributes: silty clay to clayey silt, fine to coarse silt, sandy silt to silty sand, and very fine to coarse sand. Scattered beds of volcanic ash are also present. The sand- and silt-rich beds typically display normal size grading, and most such beds are thin (<5 cm). We recorded 1112 event beds, including 30 layers of volcanic ash and 1081 inferred turbidites. A coarsening-upward trend is evident from \sim 320 to 230 mbsf, and a

prominent cluster of thick to very thick beds occurs between ~270 and 230 mbsf. The trend fines upward from ~230 to 58 mbsf and coarsens upward from ~40 mbsf to the seafloor. The overall facies character is consistent with a trench-wedge environment punctuated by frequent influxes by turbidity currents. Most of the accretionary prism at Site C0024 is represented by Lithologic Unit II.

The boundary between Lithologic Units II and III appears to be conformable and is defined by a paucity of sand beds below. Nannofossils dated as 2.06–2.45 Ma reveal no contrast in age across the unit boundary. The dominant lithology in Unit III is silty claystone to clayey siltstone. Minor lithologies include very fine sandstone, siltstone, and volcanic ash or tuff. The mud deposits originated from sustained hemipelagic settling in an outer trench-wedge setting. Silt beds were deposited from entrained layers of turbidity currents that lapped onto or spilled over the seaward slope of the trench.

The boundary between Lithologic Units III and IV appears to be conformable and is defined by the last occurrence (moving down-section) of trench-related silty turbidites. Nannofossils reveal no change in age (2.06–2.45 Ma) across the unit boundary. The boundary's position at 555 mbsf matches the top of an anomalous trend in porosity values and the top of a well-defined trend in XRD mineralogy, below which total clay minerals increase with depth (Figure F8A). The dominant lithology is bioturbated silty claystone to clayey siltstone; we also recovered six thin beds of light gray poorly lithified tuff. Sedimentation was dominated by slow hemipelagic settling in an environment that was isolated from sediment gravity flows. These environmental conditions are commonplace across the Shikoku Basin.

Structural geology

Bedding dips vary 0° – 30° (38–316 and 510–618.9 mbsf) and are slightly steeper in the shallowest part (\sim 10°–37° at 0–38 mbsf). Steep minor normal faults dipping toward the southwest and northeast are common at 0–38 mbsf, whereas the dip direction shifts toward the northwest and southeast below 100 mbsf. Deformation bands are generally dipping to the northwest or southeast, and healed faults and sediment-filled vein structures are commonly observed at 510–618.9 mbsf. A brecciated zone and a shear zone potentially corresponding to a back thrust that was imaged in the seismic reflection sections (Figure F7) were recovered at 243.5–247 and 295 mbsf, respectively.

Geochemistry

At Site C0024, the chlorinity profile displays two different trends separated by the gap in coring (Figure **F8A**). In the upper 300 m, the trend in interstitial water (IW) is from a chlorinity value similar to bottom water to one that is 2.5% less fresh at the base of this profile segment. This behavior almost certainly reflects alteration to clay minerals of reactive volcanic matter disseminated in the sediment. Below the coring gap, the trend is reversed so that a 4% freshening occurs over a narrower depth interval from 500 to 620 mbsf. The lower chlorinity profile segment suggests connection at depth with a source of lower chloride water. Another tracer of the deep fluid is the ratio of methane to higher hydrocarbons, the $C_1/(C_2 + C_3)$ ratio. This ratio decreases with depth driven in part by an increase in higher hydrocarbons (Figure **F8A**). Coupled together, these tracers suggest a fluid reservoir at depth sourced from a deeper portion of the prism where clay mineral diagenesis releases freshened waters

and thermogenic hydrocarbons are beginning to form. Unfortunately, samples from the décollement and below were not available to characterize the deeper fluids.

Physical properties

At Site C0024, physical properties measurements were conducted on core samples collected from 0 to 317.93 mbsf, 510 to 618.13 mbsf, and 652.04 mbsf. MAD measurements on discrete core samples show porosity decreases from about 55%-75% close to the seafloor to about 35% at 550 mbsf. A sharp increase in porosity to 45%-50% at 550-577 mbsf corresponds to the boundary between Lithologic Units III and IV, marking the transition into the Shikoku Basin sediments underneath. A decrease in magnetic susceptibility from 5×10^{-3} to 1.5×10^{-4} SI measured by the multisensor core logger (MSCL) is also observed around this lithologic boundary, which is consistent with the trend observed at Site C0006 upon entering the upper Shikoku Basin sediments. P-wave velocity and electrical resistivity measured on discrete samples also show a gradual decrease in velocity and resistivity around the unit boundary, which is consistent with the increase in porosity at the unit boundary. Measured thermal conductivity values generally agree with those measured at Integrated Ocean Drilling Program Sites C0006 and C0011.

Logging

Logging data for Site C0024 were acquired in Hole C0024A with a full bottom-hole assembly (BHA) (MicroScope, arcVISION, Tele-Scope, SonicScope, and seismicVISION) in the interval from seafloor to a depth of 869 mbsf (Figure F8B). Good data quality for most of the logged interval allows definition of three logging units with distinct characteristics. Resistivity, gamma ray, and *P*-wave velocity increase with depth in Logging Unit 1 (0–538.6 mbsf), and then resistivity and *P*-wave velocity show constant trends with some significant negative spikes in Logging Unit 2 (538.6–851.7 mbsf). Logging Unit 3 (851.7 mbsf to TD) is characterized by a significant decrease in resistivity. Both button and propagation resistivity show a large separation of shallow and deep resistivities over this unit, which may be affected by poor borehole conditions.

Bedding planes and fractures can be identified on resistivity images. Bedding dips mainly toward the northwest-northeast with dip angles of ~20° above 809 mbsf. Below 809 mbsf to TD, the overall bedding dips sharply increase with a mean value around 40° and a maximum close to 90° at 851 mbsf. Fractures exhibit various dip angles over the logged interval either to the north-northeast or the north-northwest. At 813 mbsf, a pair of faults dipping 15° and 20° toward the north coincide with a further drop in gamma ray, resistivity, and P-wave velocity values (Figure F9). In addition to the above log response and image observation, a synthetic seismogram using P-wave velocity and vertical seismic profile data indicates that the decrease in *P*-wave velocity values at ~806 to ~813 mbsf likely corresponds to the interpreted fault reflection in the seismic reflection volume. Our preliminary interpretation is that the onset of deformation at ~806-813 mbsf marks the top of the plate boundary fault zone. Borehole breakouts were also identified on the resistivity images throughout the hole. The orientation of the breakouts is generally consistent at 070°. Below ~600 mbsf, we observed a slight shift in breakout orientation to lower azimuths. The shift in orientation is also observed below 810 mbsf, which is 15°-20° rotation to an azimuth of ~100°.

Site C0025

Site C0025, the second riserless contingency site drilled during Expedition 358, was chosen to address questions about the timing of development of the Kumano fore-arc basin and the tectonic history of the inner accretionary wedge. The site is located where the fore-arc basin sediments are underlain by a more deformed domal or antiformal (based on seismic reflection interpretation; Figure F10) formation that is alternatively hypothesized to represent either (1) early inner wedge thrust sheet material or (2) diapiric mud rising buoyantly into place. Rotary core barrel (RCB) drilling was carried out after first washing down to 400 mbsf where coring commenced, with the objective of dating and characterizing the lower fore-arc basin and upper underlying wedge to discriminate between these hypotheses and elucidate the basin's tectonic history. Nineteen RCB cores were collected to a TD of 580.5 mbsf, and results from this site are summarized in this section (Figure F11).

Lithology

We documented the lithologic character of 18 cores from Hole C0025A and defined two lithologic units starting at 400 mbsf. The dominant lithology in Lithologic Unit I is mottled silty claystone to clayey siltstone, which we interpret to be hemipelagic mud. Thin interbeds (interpreted to be turbidites) are composed of medium to fine sandstone, silty sandstone, sandy siltstone, and siltstone. The base of Unit I at 441.93 mbsf coincides with the deepest inferred turbidite. The age range of nannofossil assemblages from Unit I is consistent with early Pleistocene deposition. The deposition of Unit I occurred during the initial stages of infilling of the Kumano forearc basin.

Bioturbated silty claystone and clayey siltstone are also common in Lithologic Unit II but are distinguished by a diverse host of secondary attributes: scattered dark green clay-rich bands; concentrations of organic matter and pyrite; foraminifers, worm tubes, sponge spicules, and Chondrites-Zoophycos trace fossils; fine sand laminae; and pumice clasts, thin volcanic ash beds, and irregular ash pods. Glauconite is distinctive as dispersed grains and in concentrated clusters. CaO (from XRF analysis) and calcite (from XRD) values increase significantly in Unit II because of higher proportions of calcareous nannofossils (Figure F11). Nannofossils from Unit II span an age range of late Miocene to early Pleistocene (1.34-4.13 Ma), and deposition probably occurred in a trench-slope environment with slow sediment accumulation rates. Unusual intervals in Cores 358-C0025A-7R, 16R, and 17R are composed of roughly equal mixtures of fine sand-, silt-, and clay-sized particles (sandy mudstone to muddy sandstone). Most such examples are unstratified, heavily fragmented, or in extreme cases, reduced to slurry. A provisional subunit boundary at 543.70 mbsf coincides with the top of one such interval.

Structural geology

The structural characteristics at Site C0025 are subhorizontal bedding planes, incohesive normal faults and cohesive (healed) faults, and sediment-filled vein structures. Inclined thick (>1 mm; sometimes >10 cm) healed faults characterized by weak clay mineral orientation and densification are observed in the lower part (Cores 358-C0025A-18R through 19R; 561.5–580.5 mbsf) (Figure F12). Unique sediment-filled vein structures with arrays oriented parallel to and sometimes continuous with the thick faults are coexisting.

Geochemistry

An important characteristic of the IW at Site C0025 is freshening by 18%–35% as observed in the salinity and chlorinity profiles (Figure F11). The minimum chlorinity value is centered at 450.3 mbsf, which coincides with the depth of the bottom-simulating reflector (BSR) inferred to represent the base of the gas hydrate stability zone, but low chlorinity extends to at least 572 mbsf. Most dissolved ions at Site C0025 do not greatly vary in concentration with depth. An important exception is boron. Boron concentrations show a broad maximum from 450.3 to 489.2 mbsf with values 2.5 times seawater. High boron coupled with freshened waters is a common signature of mud diapirs located along tectonic strike to the northeast (Kopf et al., 2003). Planned shore-based boron isotope studies may distinguish between processes related to hydrate dissociation or fluid flux from depth causing the observed chemical anomalies.

Physical properties

At Site C0025, physical properties measurements were conducted on core samples collected from 400 to 574.34 mbsf. MAD measurements on discrete core samples show an overall constant porosity trend scattering between 38.5% and 54.5% (Figure F11). Intervals with sandier formations show relatively lower porosity between 40% and 43%, and the occurrence at 544 mbsf coincides with the boundary between Lithologic Subunits IIA and IIB. Although penetrometer measurements indicate a marked increase in induration at about 465 mbsf, only a slight decrease in porosity (~3%) occurs around this depth. However, a pronounced spike in natural gamma ray count measured by MSCL occurs at this depth because of the presence of glauconite-bearing clasts found in the core. Also, the vertical anisotropy in electrical resistivity (positive when more resistive in the horizontal direction) changes from overall positive to negative at this depth (465 mbsf). Magnetic susceptibility decreases rapidly from 4×10^{-4} to 1×10^{-4} SI between 442 and 450 mbsf, which corresponds to the boundary between Lithologic Units I and II. Measured thermal conductivity values are negatively correlated with porosity and generally agree with those measured on the Kumano Basin sediments at Site C0002 (Expedition 315 Scientists, 2009; Strasser et al., 2014).

Preliminary scientific assessment

Expedition 358 had extraordinarily ambitious scientific goals, representing many firsts in scientific ocean drilling: the first sampling and in situ measurements in a plate boundary fault zone at seismogenic depths of more than 4 km to investigate and document the geology, physical and geochemical properties, and stress conditions of a plate boundary fault zone. Operationally, this required drilling ~2200 m of new depth in an existing cased hole that had already reached ~2900 mbsf, installing and cementing casing along the way, and collecting a suite of LWD logs, cuttings, downhole pressure tests, and 100-200 m of core at selected intervals. Preparation for the potential challenges of geological and stress or fluid pressure conditions in the planned borehole was intense, with several years of planning including the drill well on paper (DWOP) exercise, the implementation of a real-time geomechanics (RTG) team, and external consulting on the mud program and other parameters.

Unfortunately, we were unable to even begin to address the primary scientific objectives because of the operational difficulties encountered continuously throughout the first 4 months of riser drilling. The maximum depth achieved of 3262.5 mbsf is a new record depth for scientific ocean drilling, yet it represents only 10% of the planned advance. Even that 10% is only a partial achievement, as only cuttings and very basic logs (gamma ray and resistivity curves) were acquired to this depth. No LOTs or other downhole measurements relevant to stress and pore fluid pressure were conducted because they were planned for locations just below installed and cemented casing shoes, which were not installed. Hole C0002T cores, similarly, are the deepest ever collected, which is an operational achievement; however, they were not taken from a prioritized target zone and yielded little to no new scientific insight. Because Site C0002 riser drilling was the only primary plan for the expedition, the near-complete lack of success in achieving any scientific objectives was a striking disappointment.

Alternative contingency Sites C0024 and C0025 had specific scientific goals that were met with at least partial success. At Site C0024, the objective was to log and sample the frontal décollement zone (shallow plate boundary). The dedicated logging hole appears to have intersected at least the upper fault boundary and imaged and logged as much as 40 m of fault zone. It is not clear whether the base was reached or not. These logs add to a growing global data set of physical properties in active plate boundary fault systems. The high-resolution resistivity image log enabled analyses of borehole breakouts and orientations of planar structures in the plate boundary fault zone and overlying frontal prism. Coring efforts in Holes C0024E and C0024F to reach this zone failed, unfortunately, because of hole stability issues. However, sediments recording the transition between Shikoku Basin and trench fill sediments were successfully recovered from Hole C0024E. Shallow sediments were recovered in cores from Holes C0024B-C0024D and C0024G. The tectonic evolution of the frontal thrust system and strain partitioning between the frontal thrust and splay fault will be elucidated by stratigraphic analysis of these cores and logs, together with the results from Integrated Ocean Drilling Program Sites C0006 and C0007.

At Site C0025, the principal scientific objectives were to obtain age control on the onset of Kumano fore-arc basin filling and the nature of the deformed zone beneath it, testing alternative hypotheses of its formation through tectonic thrust faulting processes or mud diapirism. Coring from 400 to 571 mbsf yielded datable material and possible evidence for diapiric intrusion of sediments. Geochemical and other evidence suggests that older accreted material was not reached in the drilled interval.

In summary, this expedition enjoyed modest successes, mostly during the riserless contingency operations, but unfortunately did not achieve essentially any of the scientific objectives of the primary deep riser drilling plan or really get into position to tackle those objectives. This was not a result of unanticipated geological conditions such as mistaken interpretation or encountering a highly challenging drilling target; rather, the scientific hypotheses were not tested because the primary zone of interest was never reached for operational and engineering reasons.

Operations summary

Operational preparation for riser drilling

Site C0002 was the first IODP drill site where an industry-style DWOP review was held prior to the beginning of drilling. The normal complications of riser drilling are compounded by the accre-

tionary prism setting, and all parties involved in the expedition, including all third-party contractors, participated in this exercise. Expedition 358 was also the first IODP expedition where an RTG team was developed to advise the drilling team with updated evaluations of the geomechanical model. Unfortunately, drilling did not progress to a point where their expertise could be fully brought to bear on drilling evaluation.

Transit from Shimizu, Japan

Expedition 358 began on 7 October 2018 in the port of Shimizu, Japan, and the D/V *Chikyu* left on 10 October en route for Site C0002. *Chikyu* paused 2.5 days (Table T1) at the entrance of Suruga Bay to test the small-diameter RCB (SD-RCB) and RCB assembly. After completion, *Chikyu* continued on to Site C0002, arriving on 13 October.

Site C0002

Upon return to Site C0002 (Figure F1), the ship was set in dynamic positioning mode and the remotely operated vehicle (ROV) dove for a seabed survey and transponder deployment. Blowout preventer (BOP) running began at 2400 h (Japan Standard Time [JST]) on 14 October 2018. Troubleshooting found problems with the pressure switches, so the BOP was recovered to the surface for troubleshooting and repairs. After all the pressure switches in the blue pod were replaced, BOP running began again on 19 October. The BOP landed on the wellhead on 23 October without any more issues, and BOP pressure and function tests were completed by 25 October.

Two drill out cement (DOC) BHAs (12¼ and 10½ inch) (Table T2) were made up and run in the hole on 29 October and began drilling out the cement plug on 30 October. The 11¾ inch liner and 13¾ inch casing pressure test was good. Three shoe bond tests were run before the DOC BHA was pulled out of the hole for a scraper run. On 3 November, the wireline cement bond log tool was made up and run, logging between 2125 and 4878 m below rotary table (BRT) to check the condition of the casing-cement-formation bonding.

After rigging down the wireline tools on 4 November, preparations to run and set the whipstock assembly began with the easy drill sliding sleeve valve (EZSV) setting the plug setting tool. The EZSV was set at 4869 m BRT, and the 11¾ inch whipstock assembly was made up from 5 November and run to tag the top of the EZSV. The gyro assembly was run to ensure that the whipstock was facing the proper azimuth (N90E) to avoid intersecting Hole C0002P. However, the whipstock failed to set, so it was recovered, and a new whipstock assembly was made up and run in the hole on 8 November. The orientation surveys azimuth confirmed the whipstock orientation was between 88.2° and 86.5°, and the whipstock set by 9 November.

Milling to 4862 m BRT was finished by 10 November but was run in the hole again to complete milling to 4867 m BRT and dress the window. A FIT at the window on 12 November was good (equivalent mud weight = 1.450 specific gravity [SG]), so the second FIT was canceled. A 10% inch window mill assembly was run in the hole from 13 November but had trouble passing through the window; it was pulled out of the hole for grinding to reduce the outside diameter. The milling assembly was run in the hole and worked to 4864 m BRT by 2400 h on 15 November.

Drilling in Holes C0002Q-C0002T was extremely complicated, with multiple tracks in each hole (Figure F4), because it was difficult

to keep the BHAs in the same kick-off holes ("runs") outside the windows in the Hole C0002P casing. Details on bits and tools for each LWD run are in Table T2.

Hole C0002Q

Hole C0002Q began early on 18 November 2018 when the kick-off BHA began drilling from 4867 m BRT (Table T1). Hole C0002Q reached 4990 m BRT by 20 November and was pulled out of the hole to the surface by 21 November (Hole C0002Q Track 1 in Figure F4). After servicing the hydraulic power swivel (HPS) and traveling block, the $8\frac{1}{2}$ inch \times $12\frac{1}{4}$ inch LWD BHA with a Z-Reamer was made up and run in the hole. The LWD BHA reached the window and began reaming down from 4888 to 4909 m BRT; however, getting the BHA through the window proved difficult, so it was pulled out of the hole to run a hole-opening BHA from 25 November.

The hole-opening assembly, including arcVISION and Tele-Scope, was made up and run in the hole to 4778 m BRT. Before passing through the 4800 m BRT window, the BHA was pulled up to 4047 m BRT for a Z-Reamer function test when it was confirmed that the reamer ball seat had sheared. The BHA was pulled out of the hole to replace the Z-Reamer, and the replacement hole-opening assembly was made up and run in the hole, reaching 4845 m BRT by 28 November. LWD function tests confirmed all tools were working well, so washing/reaming down began. On 29 November at 4941 m BRT, the BHA packed off but was soon released, reaming to 4955 m BRT before pulling up to 4894 m BRT to activate the Z-Reamer. By 3 December, 4995 m BRT was reached with the average rate of penetration (ROP) never exceeding 3.3 m/h. By 7 December, 5230 m BRT was reached (Hole C0002Q Track 2 in Figure F4). The extremely low ROP was a concern, so the BHA was pulled and laid out by 9 December. A new LWD BHA, including an underreamer, was run in the hole and began drilling at 1345 h. The underreamer was activated when the reamer was at 4916 m BRT on 12 December, and the hole opened to 4928 m BRT (Hole C0002Q Track 3 in Figure F4). Poor progress and hole conditions continued, so the BHA was pulled out of the hole and laid down on 14 December to inspect the Z-Reamer underreamer. The underreamer was damaged (chipped blades, etc.), so a new kick off was planned to escape from the poor hole conditions in Hole C0002Q.

Hole C0002R

Preparations to run in the hole with a new whipstock began on 15 December 2018 (Table T1). After successfully conducting a casing pressure test, the new whipstock was run in the hole on 16 December and set at 4766 m BRT on 17 December. Milling out was completed by 20 December, with multiple milling BHAs and reciprocation through the window to ensure that the hole was clean. The new window cut from Hole C0002P was located at 4757-4763 m BRT (Figure F4). A FIT (1.46 SG) was conducted in the new window, and the milling BHA was pulled out of the hole and laid down on 20 December. Another window dressing BHA was run in the hole and reamed down to 4767 m BRT. The dressing BHA was pulled out of the hole in preparation for running the kick-off BHA. Drilling mud weight was increased from 1.37 to 1.39 SG on 24 December before drilling and sliding continued. On 25 December, drilling from 4811.5 m BRT began, reaching 4843 m BRT by 26 December. Although the kick-off BHA finally reached 4963 m BRT by 29 December, the many issues with poor borehole conditions, multiple overpulls while drilling, low ROP, and repeating overpulls and pressure spikes during reaming meant the BHA would be pulled out of the hole to the surface and laid out on 30 December. TeleScope data were downloaded while a new kick-off BHA was made up and run in the hole on 30 December.

On 31 December, the new kick-off hole began from 4963 m BRT, reaching 5052 m BRT on 3 January 2019 (Hole C0002R Track 1 in Figure F4). Reaming up and down commenced before returning the BHA to the surface to examine the mud motor, which was showing signs of failure. Once on deck, we found the top connection of the motor was overtorqued onto the crossover sub, whereas the motor itself had backed off, exposing the interior mechanism. A new LWD BHA was made up and run in the hole on 6 January. Washing and reaming down from 4744 m BRT began on 7 January; the Z-Reamer was activated at 4834 m BRT (bit depth). Reaming out the borehole and drilling a new hole from 8 January reached 4880 m BRT (Hole C0002R Track 2 in Figure F4). Hole cleaning and reaming were carried out until 9 January. The top drive torque started fluctuating and showing other signs of poor hole conditions, so the BHA was pulled out of the hole to the surface to avoid damaging the borehole. Examination showed that there was extensive damage to the bit and the underreamer; cutters were severely damaged. A new LWD BHA with a new underreamer was made up and run in the hole on 10 January. Because many tight spots were found while reaming down to 4745 m BRT, on 11 January we decided to set the 9% inch \times 11%inch expandable casing (ESET) at this depth. The LWD BHA was pulled out of the hole to the surface by 12 January, and preparation for 9% inch ESET installation was started. Running the ESET began on 13 January and reached 4818 m BRT by 14 January. Expanding the ESET was conducted after cementing, and the ESET launcher assembly was pulled out of the hole to the surface by January 15. The launcher tool showed no signs of damage. A 9.851 inch DOC BHA was made up and run to 1403 m BRT on 15 January. A pressure test of the 11% inch liner and ESET was conducted by 2000 h on 15 January and indicated that the casing was set and cemented properly. The DOC BHA reached 4791 m BRT on 16 January and started drilling out the ESET casing shoe. However, a drilling break, a sudden pressure increase (from 21.6 to 24.8 MPa), and stall (>38 kN) were observed from 4815 to 4816 m BRT, resulting in a stuck pipe at 1345 h on 16 January. Working the pipe started immediately and continued until 18 January with no sign that the drill string could be freed. A free point indicator tool was run to find a back-off point for the stuck BHA from 18 to 19 January. The back-off tool assembly was run and successfully backed off the drill pipe at 1730 h on 19 January between the 6¾ inch drill Collars 2 and 3 at 4793.75 m BRT. A fishing BHA was run down onto Collar 2 and began working the pipe until 23 January, jarring more than 400 times. Another attempt to collide the stuck drill string failed when the 58.5 mm OD gauge cutter failed to pass the inside of the drill pipe even after modification. A blind back-off operation was conducted on 27 January, but the drill string was reconnected because the back-off point was too shallow. A colliding tool was run and severed the stuck drill string at 4782 m BRT on 28 January. The collided drill pipe was pulled out of the hole and recovered to the surface on 29 January.

Hole C0002S

A new kick off above the fish in Hole C0002R was begun on 30 January after rig repair. A whipstock and Tri-Mill assembly were made up and run in the hole on 31 January 2019 (Table **T1**). The whipstock was set at 4779 m BRT (above the fish) and oriented at $\sim\!73^\circ$ on 1 February. Milling and dressing the casing was completed on 3 February with the window opened at 4769–4775 m BRT (Figure **F4**). An $8\frac{1}{2}$ inch kick-off BHA (bent angle 1.5°) was made up and run in the hole on 3 February.

Hole C0002S was reamed and drilled down to 4788.5 m BRT by 3 February, and then the BHA was pulled out of the hole to 4766 m BRT. A gyro assembly was run (4115 m BRT; wireline [WL] depth) to orient the BHA tool face to ~215° on 4 February. After washing and reaming down to 4788 m BRT, the BHA was recovered to the surface on 5 February. A full suite 8½ inch LWD BHA was made up (Table T1) and run in the hole to 4747 m BRT. After several LWD tool communication tests, the LWD BHA was washed down to 4780.5 m BRT. Drilling down from there began on 6 February and reached 4900 m BRT by 8 February (Figure F4). Several stalls occurred (4798, 4801.5, 4803.3, and 4805 m BRT) while drilling. Drilling resumed after activating the rotary steerable system (RSS) to reduce inclination on 8 February, but issues with miscommunication between the RSS and the lower C-Link and abnormal on/off bottom torque and pressure were observed. The RSS LWD BHA was pulled out of the hole on 8 February. Upon recovery of the BHA to the surface on 9 February, the bottom part of the BHA, the C-Link and RSS, were lost in the hole. Three fishing operations were attempted but failed. Another kick off to begin coring started with another kick-off cementing job at 4850 m BRT on 13 February (Figure F4). A new 8½ inch kick-off BHA was run and tagged the top of cement at 4748 m BRT on 15 February and then started to drill out cement.

Hole C0002T

A wireline gyro assembly was run to 4724 m BRT (WL depth) to set the orientation of the kick-off BHA at ~211° on 16 February 2019. The kick-off BHA slid from 4784 to 4800 m BRT and then drilled down to 4804 m BRT by 16 February. Fracseal (10 m3) was spotted at the hole bottom, and reaming between 4804 and 4790 m BRT was finished before the kick-off BHA was pulled out of the hole to the surface on 17 February. A coring 81/2 inch SD-RCB BHA was run to 4752 m BRT on 18 February and then washed/reamed down from 4752 to 4804 m BRT with the center bit. The center bit was recovered to the surface on 18 February, and then core cutting began from 4804 m BRT on 18 February. Three cores were cut and retrieved from 4804 to 4816 m BRT by 0300 h on 20 February (Figure F4). However, stalling and pack offs occurred at 4816 m BRT while reaming down on 20 February. The poor hole conditions required abandoning the hole, and the BHA was pulled out of the hole on 20 February and recovered to the surface on 21 February.

Three attempts at spotting a cement spot plug finally succeeded at 4769 m BRT on 24 February. This cement plug passed a pressure test on 25 February. A fourth plug back cementing job was set at 3350 m BRT by 2330 h. The diverter assembly was pulled out of the hole, and inhibited mud was spotted. A short pause for rig servicing occurred before the wear bushing and wear bushing running/retrieving tools were recovered on the surface. The riser mud was displaced with seawater before operations to recover the riser, and BOP commenced from 27 February. The riser was laid out, and the BOP was recovered in the moonpool by 2 March.

Site C0024

Site C0024 is located near the deformation front of the Nankai accretionary prism off the Kii Peninsula (Figures F1, F2, F7, F13). Understanding the function of the frontal décollement in coseismic and interseismic periods is a specific target for the drilling sites around the deformation front.

Hole C0024A

The LWD BHA was spudded in and washed down from 6 March 2019 after a seafloor survey with the underwater TV (UWTV) cam-

era. After recovering the UWTV, drilling began, pausing for surveys almost every stand. Nonstop driller connections per stand started from 8 March. After reaching 4738 m BRT on 9 March, worsening connections resulted in halting any advance. While pulling out of the hole, the LWD BHA was stopped for periodic check shots for the seismicVISION tool, performing repeat logs from 4180 to 4130 m BRT and from 3885 to 3867 m BRT. The BHA was laid out on deck by 10 March.

Holes C0024B-C0024D

After a waiting on weather break, the 10% inch hydraulic piston coring system (HPCS)/extended punch coring system (EPCS)/extended shoe coring system (ESCS) BHA (Table T3) was made up and run in the hole. *Chikyu* shifted 40 m to begin coring; a series of overpull events required the drawworks assist to recover the inner barrel, pulling the BHA above the seafloor. This resulted in Holes C0024B–C0024D. In Hole C0024D, the formation was hard enough to confirm that the same hole was being reentered by the BHA. HPCS coring was replaced in succession by EPCS, ESCS, EPCS, and finally ESCS coring. Coring continued until the inner barrel pull bar broke on recovery, and on 13 March 2019, coring in this hole was abandoned.

Hole C0024E

Hole C0024E was spudded in from 0315 h on 15 March 2019 with the 10% inch RCB BHA (Table T3). Drilling ahead to 4382 m BRT was completed by 16 March when the center bit was recovered and RCB coring began (see Table T4 for coring summary). Coring continued for 13 cores until hole conditions reached a point where reaming failed to improve things. RCB coring was stopped, and the BHA was pulled out of the hole to 111 m above the seafloor by the morning of 18 March.

Hole C0024F

The Hole C0024E RCB BHA was shifted over to spud in Hole C0024F on the evening of 18 March 2019. Drilling ahead with the center bit continued until reaching 4589.5 m BRT with few issues, but below that stand pipe pressure, HPS, overtorque, and overpull steadily worsened. The BHA was pulled out of the hole to 4553 m BRT, and pumping to clear the hole began before pulling the center bit to start coring on 21 March. By evening the borehole had worsened, and the BHA was pulled out of the hole to the surface and laid down. A "ghost core" was recovered from the core liner.

Hole C0024G

The RCB BHA was switched to the ESCS BHA and spudded in Hole C0024G on 22 March 2019. After drilling to 3971.5 m BRT, ESCS coring began, and the target depth was reached at 4191 m BRT on 25 March (Table **T4**). Transponders were recovered by the watch boat so that the ship could begin shifting to Site C0025 by 2100 h on 25 March.

Site C0025

Upon completion of drilling operations at Site C0024, *Chikyu* moved to the northwest margin of the Kumano Basin to examine the processes of the accretionary prism and fore-arc basin development.

Hole C0025A

The RCB coring BHA was made up and spudded in Hole C0025A on 25 March 2019 (Figure **F14**; Tables **T5**, **T6**). Washing down and then drilling ahead with the center bit to 2439.5 m BRT

was completed by 27 March. Coring operations continued here until the end of contingency time at 1100 h on 29 March. Coring reached 2620 m BRT, collecting 19 RCB cores (Table T7). The coring BHA was pulled out of the hole and laid down, cement was spotted in the hole, and *Chikyu* began the transit back to the port of Shimizu, Japan, reaching the anchorage on the morning of 31 March.

References

Araki, E., Saffer, D.M, Kopf, A.J., Wallace, L.M., Kimura, T., Machida, Y., Ide, S., Davis, E., and IODP Expedition 365 Shipboard Scientists, 2017. Recurring and triggered slow-slip events near the trench at the Nankai Trough subduction megathrust. *Science*, 356(6343):1157–1160.

https://doi.org/10.1126/science.aan3120

Expedition 314 Scientists, 2009. Expedition 314 Site C0002. In Kinoshita, M., Tobin, H., Ashi, J., Kimura, G., Lallemant, S., Screaton, E.J., Curewitz, D., Masago, H., Moe, K.T., and the Expedition 314/315/316 Scientists, Proceedings of the Integrated Ocean Drilling Program, 314/315/316: Washington, DC (Integrated Ocean Drilling Program Management International, Inc.).

https://doi.org/10.2204/iodp.proc.314315316.114.2009

Expedition 315 Scientists, 2009. Expedition 315 Site C0002. In Kinoshita, M., Tobin, H., Ashi, J., Kimura, G., Lallemant, S., Screaton, E.J., Curewitz, D., Masago, H., Moe, K.T., and the Expedition 314/315/316 Scientists, Proceedings of the Integrated Ocean Drilling Program, 314/315/316: Washington, DC (Integrated Ocean Drilling Program Management International, Inc.).

https://doi.org/10.2204/iodp.proc.314315316.124.2009

Kopf, A., Mora, G., Deyhle, A., Frape, S., and Hesse, R., 2003. Fluid geochemistry in the Japan Trench forearc (ODP Leg 186): a synthesis. *In Suyehiro*, K., Sacks, I.S., Acton, G.D., and Oda, M. (Eds.), *Proceedings of the Ocean Drilling Program, Scientific Results*, 186: College Station, TX (Ocean Drilling Program), 1–23.

https://doi.org/10.2973/odp.proc.sr.186.117.2003

Obara, K., and Kato, A., 2016. Connecting slow earthquakes to huge earthquakes. *Science*, 353(6296):253–257.

https://doi.org/10.1126/science.aaf1512

Strasser, M., Dugan, B., Kanagawa, K., Moore, G.F., Toczko, S., Maeda, L., Kido, Y., Moe, K.T., Sanada, Y., Esteban, L., Fabbri, O., Geersen, J., Hammerschmidt, S., Hayashi, H., Heirman, K., Hüpers, A., Jurado Rodriguez, M.J., Kameo, K., Kanamatsu, T., Kitajima, H., Masuda, H., Milliken, K., Mishra, R., Motoyama, I., Olcott, K., Oohashi, K., Pickering, K.T., Ramirez, S.G., Rashid, H., Sawyer, D., Schleicher, A., Shan, Y., Skarbek, R., Song, I., Takeshita, T., Toki, T., Tudge, J., Webb, S., Wilson, D.J., Wu, H.-Y., and Yamaguchi, A., 2014. Site C0002. *In* Strasser, M., Dugan, B., Kanagawa, K., Moore, G.F., Toczko, S., Maeda, L., and the Expedition 338 Scientists, *Proceedings of the Integrated Ocean Drilling Program*, 338: Yokohama (Integrated Ocean Drilling Program). https://doi.org/10.2204/iodp.proc.338.103.2014

Tobin, H.J., and Kinoshita, M., 2006. NanTroSEIZE: the IODP Nankai Trough Seismogenic Zone Experiment. *Scientific Drilling*, 2:23–27. https://doi.org/10.2204/iodp.sd.2.06.2006

Tobin, H., Hirose, T., Saffer, D., Toczko, S., Maeda, L., Kubo, Y., Boston, B., Broderick, A., Brown, K., Crespo-Blanc, A., Even, E., Fuchida, S., Fukuchi, R., Hammerschmidt, S., Henry, P., Josh, M., Jurado, M.J., Kitajima, H., Kitamura, M., Maia, A., Otsubo, M., Sample, J., Schleicher, A., Sone, H., Song, C., Valdez, R., Yamamoto, Y., Yang, K., Sanada, Y., Kido, Y., and Hamada, Y., 2015a. Expedition 348 summary. *In* Tobin, H., Hirose, T., Saffer, D., Toczko, S., Maeda, L., Kubo, Y., and the Expedition 348 Scientists, *Proceedings of the Integrated Ocean Drilling Program*, 348: College Station, TX (Integrated Ocean Drilling Program).

https://doi.org/10.2204/iodp.proc.348.101.2015

Tobin, H., Hirose, T., Saffer, D., Toczko, S., Maeda, L., Kubo, Y., Boston, B., Broderick, A., Brown, K., Crespo-Blanc, A., Even, E., Fuchida, S., Fukuchi, R., Hammerschmidt, S., Henry, P., Josh, M., Jurado, M.J., Kitajima, H., Kitamura, M., Maia, A., Otsubo, M., Sample, J., Schleicher, A., Sone, H., Song, C., Valdez, R., Yamamoto, Y., Yang, K., Sanada, Y., Kido, Y., and Hamada, Y., 2015b. Site C0002. *In* Tobin, H., Hirose, T., Saffer, D., Toczko, S., Maeda, L., Kubo, Y., and the Expedition 348 Scientists, *Proceedings of the Integrated Ocean Drilling Program*, 348: College Station, TX (Integrated Ocean Drilling Program).

https://doi.org/10.2204/iodp.proc.348.103.2015

Tobin, H.J, Kimura, G., and Kodaira, S., 2019. Processes governing giant subduction earthquakes: IODP drilling to sample and instrument subduction zone megathrusts. *Oceanography*, 32(1):80–93. https://doi.org/10.5670/oceanog.2019.125

Ujiie, K., and Kimura, G., 2014. Earthquake faulting in subduction zones: insights from fault rocks in accretionary prisms. *Progress in Earth and Planetary Science*, 1:7–37. https://doi.org/10.1186/2197-4284-1-7

Underwood, M.B., and Moore, G.F., 2012. Evolution of sedimentary environments in the subduction zone of southwest Japan: recent results from the NanTroSEIZE Kumano Transect. *In* Busby, C., and Azor, A. (Eds.), *Tectonics of Sedimentary Basins: Recent Advances*: New York (Wiley-Blackwell), 310–326. https://doi.org/10.1002/9781444347166.ch15

Table T1. Expedition 358 drilling summary, Sites C0002, C0024, and C0025. * = hole top is top of whipstock window depth, † = hole top is start depth of kick off from Hole C0002S. BRT = below rotary table, MSL = from mean sea level. — = not applicable. LWD = logging while drilling, MWD = measurement while drilling.

			Water	depth	Depth	(mbsf)	Depth	BRT (m)
Hole	Latitude	Longitude	BRT (m)	MSL (m)	Тор	Bottom	Тор	Bottom
C0002Q*	33°18′30.4200″N	136°38′12.1740″E	1967.5	1939.0	2887.3	3262.5	4854.8	5230.0
C0002R*	33°18′30.4200″N	136°38′12.1740″E	1967.5	1939.0	2789.5	2995.5	4757.0	4963.0
C0002S*	33°18′30.4200″N	136°38′12.1740″E	1967.5	1939.0	2802.1	2933.5	4769.6	4901.0
C0002T [†]	33°18′30.4200″N	136°38′12.1740″E	1967.5	1939.0	2816.5	2848.5	4784.0	4816.0
C0024A	33°02′02.6379″N	136°47′23.9464″E	3870.0	3841.5	0.0	869.0	3870.0	4739.0
C0024B	33°02′00.0000″N	136°47′23.7960″E	3872.0	3843.5	0.0	6.0	3872.0	3878.0
C0024C	33°02′00.0000″N	136°47′23.7960″E	3872.0	3843.5	6.0	7.0	3878.0	3879.0
C0024D	33°02′00.0000″N	136°47′23.7960″E	3872.0	3843.5	7.0	128.0	3879.0	4000.0
C0024E	33°02′00.0000″N	136°47′23.7960″E	3872.0	3843.5	0.0	625.5	3872.0	4497.5
C0024F	33°02′03.9362″N	136°47′23.9726″E	3868.0	3839.5	0.0	731.0	3868.0	4599.0
C0024G	33°02′00.6490″N	136°47′24.1800″E	3871.5	3843.0	0.0	319.5	3871.5	4191.0
C0025A	33°24′05.4600″N	136°20′09.1428″E	2039.5	2011.0	0.0	580.5	2039.5	2620.0

	Cores	Advanced	Core re	covery	 Cored interval 	Da	ite	Days in hole	
Hole	(N)	(m)	(m)	(%)	(m)	Start	Finish		
C0002Q*	_	_	_	_	LWD/MWD	17 Nov 2018	14 Dec 2018	27	
C0002R*	_	_	_	_	LWD/MWD	22 Dec 2018	29 Jan 2019	38	
C0002S*	_	_	_	_	LWD/MWD	3 Feb 2019	8 Feb 2019	5	
C0002T [†]	3	12.0	2.49	20.8	2836.5-2848.5	19 Feb 2019	21 Feb 2019	2	
C0024A	_	_	_	_	LWD/MWD	6 Mar 2019	10 Mar 2019	4	
C0024B	1	6.0	7.14	119.0	0.0-6.0	12 Mar 2019	12 Mar 2019	0	
C0024C	1	1.0	1.37	137.0	6.0-7.0	12 Mar 2019	12 Mar 2019	0	
C0024D	14	121.0	98.52	81.4	7.0-128.0	12 Mar 2019	13 Mar 2019	1	
C0024E	12	111.5	51.52	46.2	510.0-621.5	15 Mar 2019	18 Mar 2019	3	
C0024F	0	0.0	0.00	0.0	0.0	18 Mar 2019	21 Mar 2019	3	
C0024G	24	219.5	140.72	64.1	100.0-319.5	22 Mar 2019	25 Mar 2019	3	
C0025A	19	180.5	123.02	68.2	400.0-580.5	26 Mar 2019	29 Mar 2019	3	

Table T2. Bottom-hole assembly (BHA) summary, Site C0002. LWD = logging while drilling, RIH = run in hole, POOH = pull out of hole. — = not applicable. NOV = National Oilwell Varco, SLB = Schlumberger. PDC = polycrystalline diamond. XO = crossover, DP = drill pipe, DC = drill collar, NMDC = nonmagnetic drill collar, std = stand, jt = joint, CSG = casing, NSD = nonstop driller. WBRT = Wear Brush Running Tool, WBRRT = Wear Brush Running Retrieval Tool, UR = underreamer, HWDP = heavyweight drill pipe, UBHO = universal bottom hole orientation, PDM = positive displacement motor, NAMCBV = Multi Cycle Bypass Valve. SD-RCB = small-diameter rotary core barrel. (Continued on next two pages.)

No.	Hole	LWD run	RIH date	POOH date	Bit type	BHA type	BHA details
1	C0002P	_	25 Oct 2018	26 Oct 2018	NA	13-3/8 inch WBRT	Jetting sub \times XO \times 5-1/2 inch DP S-140 (9 std) \times XO \times WBRRT \times XO \times 5-1/2 inch DP \times S-150 6 m pup \times 5-1/2 inch DP S-150 (5 std) \times XO \times 6-5/8 inch DP Z-140 (22 std) \times 6-5/8 inch DP UD-165
2	C0002P	_	26 Oct 2018	30 Oct 2018	Bit 1: 12-1/4 inch NOV PDC M423 A162762	12-1/4 inch Drill- Out	12-1/4 inch bit × bit sub w/float (nonported) \times 8-1/2 inch DC (4 std) \times XO \times 5-11/16 inch HWDP (3 std) \times XO \times 5-1/2 inch DP S140 (30 std) \times XO \times 5-1/2 inch DP S-150 (47 std) \times XO \times 6-5/8 inch DP UD-165
3	C0002P	_	30 Oct 2018	02 Nov 2018	Bit 2: 10-5/8 inch Smith XR+CPS 117 RJ8093	10-5/8 inch Drill- Out	10-5/8 inch bit (XR+CPS milled tooth) \times bit sub w/float \times XO \times 6 3/4 inch DC (3 std) \times 6-1/2 inch jar \times 6-3/4 inch DC (1 std) \times XO \times 5-11/16 inch HWDP (3 std) \times XO \times 5-1/2 inch DP S140 (16 std) \times XO \times 5-1/2 inch DP S150 (56 std) \times XO \times 6-5/8 inch DP Z140 (22 std) \times 6-5/8 inch DP UD-165
4	C0002P	_	02 Nov 2018	03 Nov 2018	Bit 4: 10-5/8 inch Smith XR+CPS 117 JR8093	Scraper	10-5/8 inch bit × bit sub w/float × 11-3/4 inch CSG scraper × 10-5/8 inch stabilizer × 8-1/2 inch DC (1 jt) × 10-5/8 inch stabilizer × 8-1/2 inch DC (9 jt) × XO-1 × 5 inch DP S-140 (15 std) × 5-1/2 inch DP S-140 (9 std) × XO-2 × 13-3/8 inch CSG scraper × XO-3 × 5-1/2 inch DP S-150 (51 std) × XO-4 × 6-5/8 inch DP Z-140 (22 std) × 6-5/8 inch DP UD-165
5	C0002P	_	05 Nov 2018	08 Nov 2018	10-5/8 inch SLB Tri-Mill	Whipstock	Anchor/Whipstock assembly \times 10-5/8 inch DP Trill Mill \times 8 inch OD running tool \times 6-5/8 inch HWDP (1 jt provided by SLB) \times NAMCBV \times XO-1 \times 8 inch UBHO sub \times XO-2 \times XO-3 \times 8-1/2 inch coring DC (4 std) \times XO-4 \times 5-11/16 inch HWDP (3 std) \times Churchill drift catcher sub \times XO-55 \times 5 inch DP S-140 (23 std) \times XO-6 \times 5-1/2 inch DP S-150 (50 std) \times XO-7 \times 6-5/8 inch DP Z-140 (22 std) \times 6-5/8 inch DP UD-165
6	C0002Q	_	08 Nov 2018	11 Nov 2018	10-5/8 inch SLB Tri-Mill	Whipstock	Anchor/Whipstock assembly \times 10-5/8 inch DP Trill Mill \times 8 inch OD running tool \times 6-5/8 inch HWDP (1 jt provided by SLB) \times XO-1 \times 8 inch UBHO sub \times XO-2 \times XO-3 \times 8-1/2 inch coring DC (4 std) \times XO-4 \times 5-11/16 inch HWDP (3 std) \times Churchill drift catcher sub \times XO-5 \times 5 inch DP S-140 (23 std) \times XO-6 \times 5-1/2 inch DP S-150 (50 std) \times XO-7 \times 6-5/8 inch DP Z-140 (22 std) \times 6-5/8 inch DP UD-165
7	C0002Q	_	11 Nov 2018	13 Nov 2018	10-5/8 inch SLB Tri-Mill	Whipstock	Anchor/Whipstock assembly \times 10-5/8 inch DP Trill Mill \times 8 inch OD Running Tool \times 6-5/8 inch HWDP (1 jt provided by SLB) \times XO-1 \times 8 inch UBHO sub \times XO-2 \times XO-3 \times 8-1/2 inch coring DC (4 std) \times XO-4 \times 5-11/16 inch HWDP (3 std) \times Churchill drift catcher sub \times XO-5 \times 5 inch DP S-140 (23 std) \times XO-6 \times 5-1/2 inch DP S-150 (50 std) \times XO-7 \times 6-5/8 inch DP Z-140 (22 std) \times 6-5/8 inch DP UD-165
8	C0002Q	_	13 Nov 2018	14 Nov 2018	10-5/8 inch SLB Window mill	Window Mill	10-5/8 inch Window mill \times XO-1 \times 10-5/8 inch String mill \times 10-5/8 inch String mill \times XO-2 \times float sub w/float \times 8-1/2 inch drilling DC (4 std) \times XO-3 \times 5-11/16 inch HWDP (3 std) \times XO-4 \times 5 inch DP S-140 (23 std) \times XO-5 \times 5-1/2 inch DP S-150 (50 std) \times XO-6 \times 6-5/8 inch DP Z-140 (22 std) \times 6-5/8 inch DP UD-165
9	C0002Q	_	14 Nov 2018	16 Nov 2018	10-5/8 inch SLB Window mill	Window Mill	10-5/8 inch Window mill \times XO-1 \times 10-5/8 inch String mill \times XO-2 \times XO-3 \times 6-5/8 inch HWDP \times XO-4 \times XO-5 \times float sub w/float \times 8-1/2 inch drilling DC (4 std) \times XO-6 \times 5-11/16 inch HWDP (3 std) \times XO-7 \times 5 inch DP S-140 (23 std) \times XO-8 \times 5-1/2 inch DP S-150 (50 std) \times XO-9 \times 6-5/8 inch DP Z-140 (22 std) \times 6-5/8 inch DP UD-165
10	C0002Q	1	17 Nov 2018	21 Nov 2018	Bit 3: 8-1/2 inch Smith XR+N 117 RJB198	8-1/2 inch Kick- Off	8-1/2 inch bit × motor (w/1.5° bent angle) × 8-1/8 inch stab (SLB) × float sub w/float × 6-3/4 inch pony NMDC × XO × TeleScope 675 × 6-3/4 inch NMDC × 6-3/4 inch UBHO × 6-3/4 inch DC (3 std) × 6-1/2 inch jar × 6-3/4 inch DC (2 jt) × XO × 5-1/16 inch HWDP (3 std) × XO × 5-1/2 inch DP S-140 (25 std) × XO × 5-1/2 inch DP S-140 (25 std) × XO × 5-1/2 inch DP S-140 (25 std) × 6-5/8 inch DP UD-165 with NSD
11	C0002Q	2	22 Nov 2018	25 Nov 2018	Bit 4: 8-1/2 inch Smith Axeblade X616 M323 QF3233	8-1/2 inch × 12- 1/4 inch LWD w/UR	8-1/2 inch bit × MicroScope 675 × arcVISION 675 × TeleScope 675 × SonicScope 675 × seismicVISION 675 × XO × 6-3/4 inch DC (1) × Z-reamer × float sub (nonported float) × 7 inch well commander × XO × 8-1/2 inch DC (1) × 10-1/4 inch stab × 8-1/2 inch DC (3 std) × 8 inch jar × 8-1/2 inch DC (2) × XO × 5-11/16 inch HWDP (3 std) × XO
12	C0002Q	3	25 Nov 2018	27 Nov 2018	Bit RR4a: 8-1/2 inch Smith Axeblade X616 M323 QF3233	8-1/2 inch × 12- 1/4 inch Hole- Opening	8-1/2 inch bit × bit sub × arcVISION 675 × TeleScope 675 × XO × 8-1/4 inch stabilizer × 6-3/4 inch DC (1) × Z-reamer × float sub w/ported float × 6-3/4 inch DC (11) × XO × 6-3/4 inch coring DC (3) × XO × 8-1/2 inch DC (3) × 8 inch jar × 8-1/2 inch DC (3) × XO × 5-11/16 inch HWDP (3 std) × XO

Table T2 (continued). (Continued on next page.)

No.	Hole	LWD run	RIH date	POOH date	Bit type	BHA type	BHA details
13	C0002Q	4	27 Nov 2018	09 Dec 2018	Bit RR4b: 8-1/2 inch Smith Axeblade X616 M323 QF3233	8-1/2 inch × 12- 1/4 inch Hole- Opening	8-1/2 inch bit × bit sub (nonported) × XO × arcVISION 675 × TeleScope 675 × XO × 8-1/4 inch stabilizer × 6-3/4 inch DC (1) × Z-reamer × float sub (nonported float) × 6-3/4 inch DC (11) × XO × 6-3/4 inch coring DC (3) × XO × 8-1/2 inch DC (3) × 8 inch jar × 8-1/2 inch DC (3) × XO × 5-11/16 inch HWDP (3 std) × XO
14	C0002Q	5	9 Dec 2018	14 Dec 2018	Bit 5: 8-1/2 inch Smith Axeblade XS616 M323 QF3237	8-1/2 inch × 12- 1/4 inch LWD	8-1/2 inch bit × bit sub (nonported) × XO × arcVISION 675 × TeleScope 675 × XO × 8-1/4 inch stabilizer × 6-3/4 inch DC (1) × Z-reamer × float sub (nonported float) × 6-3/4 inch DC (1) × 8-1/8 inch stabilizer × 6-3/4 inch DC (10) × XO × 8-1/2 inch DC (3) × 10-5/8 inch stabilizer × 8-1/2 inch DC (3) × 8 inch jar × 8-1/2 inch DC (3) × XO × 5-11/16 inch HWDP (3 std) × XO
15	C0002R	_	16 Dec 2018	18 Dec 218	10-1/2 inch Tri- Mill	Whipstock	Anchor/Whipstock assembly × 10-1/2 inch OD Trill Mill × 8 inch OD running tool × 6-5/8 inch HWDP (1 jt, provided by SLB) × XO-1 × XO-2 × XO-3 × 8-1/2 inch coring DC (4 std) × XO-4 × 5 11/16 inch HWDP (3 std) × XO-5 × 5 inch DP S-140 (23 std) × XO-6 × 5-1/2 inch DP S-150 (70 std) × XO-7 × 6-5/8 inch DP Z-140 (22 std) × 6-5/8 inch DP UD-165
16	C0002R	_	18 Dec 2018	20 Dec 2018	10-1/2 inch Tri- Mill	10-1/2 inch Tri-Mill	10-1/2 inch OD Trill Mill \times 8 inch OD running tool \times 6-5/8 inch HWDP (1 jt, provided by SLB) \times XO-1 \times XO-2 \times float sub (nonported float) \times XO-3 \times XO-4 \times 8-1/2 inch coring DC (4 std) \times XO-4 \times 5-11/16 inch HWDP (3 std) \times XO-5 \times 5 inch DP S-140 (23 std) \times XO-6 \times 5-1/2 inch DP S-150 (70 std) \times XO-7 \times 6-5/8 inch DP Z-140 (22 std) \times 6-5/8 inch DP UD-165
17	C0002R	_	20 Dec 2018	22 Dec 2018	10-5/8 inch Window Mill	10-5/8 inch Window Mill	10-5/8 inch Window mill \times XO-1 w/float (nonported) \times 10-5/8 inch String mill \times XO-2 \times XO-3 \times 6-5/8 inch HWDP \times XO-4 \times 8 1/2 inch drilling DC (4 std) \times XO-5 \times 5-11/16 inch HWDP (3 std) \times XO-6 \times 5 inch DP S-140 (23 std) \times XO-7 \times 5-1/2 inch DP S-150 (70 std) \times XO-8 \times 6-5/8 inch DP Z-140 (22 std) \times 6-5/8 inch DP UD-165
18	C0002R	1	22 Dec 2018	30 Dec 2018	Bit 6: 8-1/2 inch Smith FHKi28ODVPS 527X RG2023	8-1/2 inch Kick- Off	8-1/2 inch bit × A675XP PDM with 1.15° bend × 8-1/8 inch stab (SLB) × float sub (nonported float valve) (SLB) × 6-3/4 inch pony NMDC × XO-1 × TeleScope 675 × XO-2 × 6-3/4 inch NMDC × 6-3/4 inch DC (3 std) × 6-1/2 inch jar × 6-3/4 inch DC (2 jt) × XO-3 × 5-11/2 inch DP (3 std) × XO-4 × 5-1/2 inch DP S-140 (25 std) × XO-5 × 5-1/2 inch DP S-150 (65 std) × XO-6 × 6-5/8 inch DP Z-140 (22 std) × 6-5/8 inch DP UD-165
19	C0002R	2	30 Dec 2018	05 Jan 2019	Bit 7: 8-1/2 inch Smith XR+N 117 RJ8199	8-1/2 inch Kick- Off	8-1/2 inch bit × A675XP PDM with 1.50° bend × 8-1/4 inch stab (SLB) × float sub (nonported float valve) (SLB) × 6-3/4 inch pony NMDC × XO-1 × TeleScope 675 × XO-2 × 6-3/4 inch NMDC × 6-3/4 inch DC (3 std) × 6-1/2 inch jar × 6-3/4 inch DC (2 jt) × XO-3 × 5-11/16 inch HWDP (3 std) × XO-4 × 5-1/2 inch DP S-140 (25 std) × XO-5 × 5-1/2 inch DP S-150 (63 std) × XO-6 × 6-5/8 inch DP Z-140 (23 std) × 6-5/8 inch DP UD-165
20	C0002R	3	6 Jan 2019	09 Jan 2019	Bit 8: 8-1/2 inch Smith MDi516UBPXG M223 QF3591	8-1/2 inch × 12- 1/4 inch LWD	8-1/2 inch bit × bit sub (nonported float) × XO-1 × arcVISION 675 × TeleScope 675 (w/IWOB, 700 gpm setting) × XO-2 × XO 3 × 8-1/4 inch stabilizer × 6-3/4 inch DC (1) × Z-reamer × float sub (nonported float) × 6-3/4 inch DC (4-1/2 IF) (1) × 8-1/8 inch stabilizer × XO-4 × 6-3/4 inch DC (4 IF) (10) × XO-5 × 6-3/4 inch DC (4-1/2 IF) (7) × 6-1/2 inch jar × 6-3/4 inch j
21	C0002R	4	10 Jan 2019	12 Jan 2019	Bit 9: 8-1/2 inch Smith FHKi28ODVPS 527X RG1529	8-1/2 inch × 12- 1/4 inch LWD	8-1/2 inch bit (new) × bit sub (nonported float valve) × XO-1 × Z-reamer (or HRR8000) × XO-2 × arcVISION 675 × TeleScope 675 × XO-3 × XO-4 × 10-5/8 inch stabilizer × XO-5 × 6-3/4 inch DC (4-1/2 IF) (3) × XO-6 × XO-7 × 8-1/2 inch DC (3 std) × 8 inch jar × 8-1/2 inch DC (1 std) × XO-8 × 5-11/16 inch HWDP (3 std) × Churchill drift sub × XO-9 × 5 inch DP S140 (12 std) × 5-1/2 inch DP S-140 (22 std) × XO-10 × 5-1/2 inch DP S-150 (70 std) × XO-11 × 6-5/8 inch DP Z-140 (12 std) × 6-5/8 inch DP UD-165 NSD stand
NA	C0002R	_	12 Jan 2019	15 Jan 2019	NA	9-5/8 inch × 11- 3/4 inch ESET	Launcher assembly \times 9-5/8 inch \times 11-3/4 inch ESET (20 jt) \times
			12 Jan 2019	15 Jan 2019		Inner string	anchor hanger × taper guide Safety joint × XO-1 × debris catcher (2 jt) × XO-2 × 5 inch DP S140 (3 m pup) × 5 inch DP S140 (5 std) × XO-4 × debris catcher (1 jt) × XO-5 × 5 inch DP S140 (7 std) × 5-1/2 inch DP S140 (22 std) × XO-7 × 5-1/2 inch DP S-150 (70 std) × XO-8 × 6 5/8 inch DP Z-140 (22 std) × 6-5/8 inch DP UD-165
22	C0002R	_	15 Jan 2019	20 Jan 2019	9.851 inch Junk Mill	9.851 inch Drill- Out	9.851 inch junk mill × bit sub w/float (nonported) × XO-1 × 6-3/4 inch DC (4-1/2 IF) (3 std) × 6-1/2 inch jar × 6-3/4 inch DC (4-1/2 IF) (2 jt) × XO-2 × Churchill drift sub × 5 inch DP S-140 (12 std) × 5-1/2 inch DP S-140 (22 std) × XO-3 × 5-1/2 inch DP S-150 (70 std) × XO-4 × 6-5/8 inch DP Z140 (12 std) × 6-5/8 inch DP UD-165
23	C0002R	_	20 Jan 2019	29 Jan 2019	NA	Fishing	Screw-in sub (4-1/2 IF pin \times 4-1/2 IF box) \times XO-1 \times XO-2 \times 8 inch

Table T2 (continued).

No.	Hole	LWD run	RIH date	POOH date	Bit type	BHA type	BHA details
24	C0002S	_	31 Jan 2019	03 Feb 2019	9-3/4 inch Tri-Mill	Whipstock	10-3/4 inch Whipstock × 9-3/4 inch Tri-Mill × 6-1/2 inch OD running tool × XO × 5-11/16 inch HWDP × XO × 6-1/2 inch UBHO × XO × 6-3/4 inch coring DC (9) × XO × XO × 7 inch coring DC (12) × XO × XO × 5-11/16 inch HWDP (12) × XO
25	C0002S	1	03 Feb 2019	05 Feb 2019	Bit 10: 8-1/2 inch Smith FHK30ODPS 536 RG1504	8-1/2 inch Kick- Off	8-1/2 inch bit × motor (A675XP w/1.15 bent angle) w/8-3/8 inch stab × 8-1/8 inch stab × float sub (nonported float) × 6-3/4 inch pony NMDC × XO × TeleScope 675 w/IWOB × XO × 6-3/4 inch NMDC × 6-1/2 inch UBHO × XO × 6-3/4 inch coring DC (3) × XO × 6-3/4 inch DC (4-1/2 IF) (6) × 6-1/2 inch jar × 6-3/4 inch DC (4-1/2 IF) (2) × XO × 5-11/16 inch HWDP × XO
26	C0002S	2	05 Feb 2019	08 Feb 2019	Bit 11: 8-1/2 inch Smith XZ2716 M323 QF3395	8-1/2 inch LWD	$8-1/2\ inch\ bit \times Xceed\ 675 \times lower\ C-Link\ 675 \times XO \times filter\ sub \times mud\ motor\ (675ERT7850) \times float\ sub\ (nonported\ float) \times upper\ C-Link\ 675 \times MicroScope\ 675 \times ARC-6 \times TeleScope\ 675 \times SonicScope\ 675 \times seismicVISION\ 675 \times XO \times XO \times 6-3/4\ inch\ DC\ (4\ IF)\ (3\ std) \times XO \times 6-3/4\ inch\ DC\ (2\ std) \times 6-1/2\ inch\ jar \times 6-3/4\ inch\ DC\ (2\ jt) \times XO \times 5-11/16\ inch\ HWDP\ (3\ std) \times XO$
27	C0002S	_			NA	Fishing	8-1/2 inch bit \times Xceed 675 \times Lower C-link bottom sub
			08 Feb 2019	10 Feb 2019		Fishing	8-1/8 inch OD overshot × fishing bumper sub × 6-3/4 inch fishing jar × XO × 8-1/8 inch stab (SLB) × XO × 6-3/4 inch DC (4 IF) (3 std) × XO × 5-11/16 inch HWDP (3 std) × XO
28	C0002S	_	10 Feb 2019	12 Feb 2019	NA	Diverter	7 inch diverter
29	C0002S	_	12 Feb 2019	14 Feb 2019	NA	Fishing	8-1/8 inch OD overshot \times fishing bumper sub \times 6-3/4 inch fishing jar \times XO \times 8-1/8 inch stabilizer (SLB) \times XO \times 6-3/4 inch DC (4-1/2 IF) (1 std) \times XO
30	C0002T	_	14 Feb 2019	16 Feb 2019	RR10a 8-1/2 inch Smith FHK30ODPS 537 RG1504	8-1/2 inch Kick- Off	8-1/2 inch bit × motor (1.50° bend) × float sub (nonported float) × 6-3/4 inch pony NMDC × XO-1 × TeleScope 675 × XO-2 × 6-3/4 inch UBHO × 6-3/4 inch NMDC × XO-3 × 6-3/4 inch coring DC (1 std) × XO-4 × 6-3/4 inch DC (2 std) × 6-1/2 inch jar × 6-3/4 inch DC (2 jt) × XO-5 × 5-11/16 inch HWDP (3 std) × XO-6
31	C0002T	_	16 Feb 2019	21 Feb 2019	Bit 12: 8-1/2 inch Baker BHC407C M333 7151964	8-1/2 inch Coring	8-1/2 inch core bit × bit sub w/8.44 inch stabilizer × SD-RCB outer barrel × landing sub w/ 8.44 inch stabilizer × head sub × 7 inch coring DC (12 jt) × XO-1 × 5-11/16 inch HWDP (3 std) × XO-2
32	C0002T	_	21 Feb 2019	26 Feb 2019	NA	Diverter	Diverter
33	C0002N	_	26 Feb 2019	27 Feb 2019	NA	WBRRT	Diverter \times XO \times 5-1/2 inch DP S150 (2 std) \times XO \times WBRRT \times XO \times 5-1/2 inch DP S150 6 m pup

Table T3. Bottom-hole assembly (BHA) summary, Site C0024. LWD = logging while drilling, RIH = run in hole, POOH = pull out of hole. — = not applicable. XO = crossover, DC = drill collar, DP = drill pipe, std = stand, jt = joint, HWDP = heavyweight drill pipe, PDC = polycrystalline diamond, SBOCB = shallow outer core barrel, CLOCB = deep outer core barrel.

No.	Hole	LWD run	RIH (2019)	POOH (2019)	Bit type	BHA type	BHA details
34	C0024A	1	4 Mar	10 Mar	Bit 13: 8-1/2 inch Smith MDi516UBPXG M223; S/N QF3594	8-1/2 inch LWD	8-1/2 inch bit × MicroScope 675 × arcVISION 675 × TeleScope 675 × SonicScope 675 × seismicVISION 675 × XO-1 × float sub (nonported) × XO-2 × 6-3/4 inch DC (4 IF) (2 std) × XO-3 × 6-3/4 inch DC (4-1/2 IF) (1 std) × 6-1/2 inch jar × 6-3/4 inch DC (1 std) × XO-4 × 5-11/16 inch HWDP (3 std)
35	C0024B C0024C C0024D	_	11 Mar 11 Mar 11 Mar	11 Mar 11 Mar 14 Mar	Bit 14: 10-5/8 inch AAI SC513 M223; S/N A2253-5-01	Shallow core	10-5/8 inch PDC bit \times bit sub w/o stabilizer \times SBOCB \times landing sub \times top sub \times head sub \times 8-1/2 inch coring DC (12 jt) \times XO
36	C0024E C0024F	_	14 Mar 18 Mar	18 Mar 21 Mar	Bit 15: 10-5/8 inch Baker BHC405; S/N 7161556	Deep core	10-5/8 inch PDC bit \times bit sub w/o stabilizer \times CLOCB \times landing sub \times top sub \times head sub \times 8-1/2 inch coring DC (9 jt) \times 8-1/2 inch coring jar \times 8-1/2 inch coring DC (3 jt) \times XO-1 \times 5-11/16 inch HWDP (3 std) \times 5-1/2 inch DP S150 (70 std) \times XO-2 \times 6-5/8 inch DP Z140 (22 std) \times 6-5/8 inch DP UD165
37	C0024G	_	22 Mar	25 Mar	Bit RR14a: AAI SC513 N223; S/N A2253-5-01	Shallow core	10-5/8 inch PDC bit \times bit sub w/o stabilizer \times SBOCB \times landing sub \times top sub \times head sub \times 8-1/2 inch coring DC (12 jt) \times XO

Table T4. Coring summary, Holes C0024B–C0024G. HPCS = hydraulic piston coring system. EPCS = extended punch coring system. ESCS = extended shoe coring system, RCB = rotary coring barrel. — = not applicable.

			Coring time _	Depth	BRT (m)	Depti	n (mbsf)		Rec	overy
Hole, core	Coring system	Time on deck (h)	(min)	Тор	Bottom	Тор	Bottom	Advanced (m)	(m)	(%)
C0024B-1H	HPCS	12 Mar 2019 0313	_	3872.0	3878.0	0.0	6.0	6.0	7.14	119.0
C0024C-1H	HPCS	12 Mar 2019 0512	_	3878.0	3879.0	6.0	7.0	1.0	1.37	137.0
C0024D-1H	HPCS	12 Mar 2019 0643	_	3879.0	3883.5	7.0	11.5	4.5	4.98	111.0
C0024D-2H	HPCS	12 Mar 2019 0858	_	3883.5	3892.5	11.5	20.5	9.0	9.68	108.0
C0024D-3H	HPCS	12 Mar 2019 1059	_	3892.5	3902.0	20.5	30.0	9.5	9.67	102.0
C0024D-4H	HPCS	12 Mar 2019 1534	_	3902.0	3908.0	30.0	36.0	6.0	9.94	165.7
C0024D-5T	EPCS	12 Mar 2019 1928	18	3908.0	3917.5	36.0	45.5	9.5	4.25	44.7
C0024D-6X	ESCS	12 Mar 2019 2203	15	3917.5	3927.0	45.5	55.0	9.5	9.70	102.1
C0024D-7T	EPCS	13 Mar 2019 0119	9	3927.0	3933.5	55.0	61.5	6.5	2.60	40.0
C0024D-8X	ESCS	13 Mar 2019 0448	21	3933.5	3943.0	61.5	71.0	9.5	6.10	64.2
C0024D-9X	ESCS	13 Mar 2019 0703	24	3943.0	3952.5	71.0	80.5	9.5	9.15	96.3
C0024D-10X	ESCS	13 Mar 2019 0854	13	3952.5	3962.0	80.5	90.0	9.5	8.24	86.7
C0024D-11X	ESCS	13 Mar 2019 1056	17	3962.0	3971.5	90.0	99.5	9.5	8.81	92.7
C0024D-12X	ESCS	13 Mar 2019 1423	19	3971.5	3981.0	99.5	109.0	9.5	7.65	80.5
C0024D-13X	ESCS	13 Mar 2019 1619	11	3981.0	3990.5	109.0	118.5	9.5	6.88	72.4
C0024D-13X	ESCS	14 Mar 2019 0454	22	3990.5	4000.0	118.5	128.0	9.5	0.87	9.2
C0024E-1R	RCB	16 Mar 2019 1054	22	4382.0	4391.5	510.0	519.5	9.5 9.5	2.43	25.6
C0024E-2R	RCB	16 Mar 2019 1422	39	4391.5	4398.5	519.5	526.5	7.0	4.47	63.9
C0024E-3R	RCB	16 Mar 2019 1843	64	4398.5	4408.0	526.5	536.0	9.5	4.90	51.6
C0024E-4R	RCB	16 Mar 2019 2248	65	4408.0	4417.5	536.0	545.5	9.5	4.23	44.5
C0024E-5R	RCB	17 Mar 2019 0247	47	4417.5	4427.0	545.5	555.0	9.5	4.91	51.7
C0024E-6R	RCB	17 Mar 2019 0639	33	4427.0	4436.5	555.0	564.5	9.5	4.64	48.8
C0024E-7R	RCB	17 Mar 2019 1053	35	4436.5	4446.0	564.5	574.0	9.5	4.63	48.7
C0024E-8R	RCB	17 Mar 2019 1428	36	4446.0	4455.5	574.0	583.5	9.5	2.87	30.2
C0024E-9R	RCB	17 Mar 2019 1829	37	4455.5	4465.0	583.5	593.0	9.5	4.55	47.9
C0024E-10R	RCB	17 Mar 2019 2153	40	4465.0	4474.5	593.0	602.5	9.5	2.93	30.8
C0024E-11R	RCB	18 Mar 2019 0138	33	4474.5	4484.0	602.5	612.0	9.5	4.17	43.9
C0024E-12R	RCB	18 Mar 2019 0543	33	4484.0	4493.5	612.0	621.5	9.5	6.79	71.5
C0024E-13G	RCB	18 Mar 2019 1230	0	4493.5	4493.5	621.5	621.5	0.0	2.39	N/A
C0024F-1G	RCB	21 Mar 2019 1945	0	4520.0	5562.0	652.0	694.0	0.0	0.12	N/A
C0024G-1X	ESCS	22 Mar 2019 2221	32	3971.5	3981.0	100.0	109.5	9.5	6.64	69.9
C0024G-2X	ESCS	23 Mar 2019 0009	26	3981.0	3990.5	109.5	119.0	9.5	6.20	65.3
C0024G-3X	ESCS	23 Mar 2019 0158	20	3990.5	4000.0	119.0	128.5	9.5	3.70	38.9
C0024G-4X	ESCS	23 Mar 2019 0340	15	4000.0	4005.5	128.5	134.0	5.5	4.60	83.6
C0024G-5X	ESCS	23 Mar 2019 0512	13	4005.5	4010.5	134.0	139.0	5.0	2.40	48.0
C0024G-6X	ESCS	23 Mar 2019 0831	25	4010.5	4020.0	139.0	148.5	9.5	5.00	52.6
C0024G-7X	ESCS	23 Mar 2019 1017	33	4020.0	4029.5	148.5	158.0	9.5	6.15	64.7
C0024G-8X	ESCS	23 Mar 2019 1206	25	4029.5	4039.0	158.0	167.5	9.5	7.85	82.6
C0024G-9X	ESCS	23 Mar 2019 1344	25	4039.0	4048.5	167.5	177.0	9.5	7.37	77.6
C0024G-10X	ESCS	23 Mar 2019 1635	29	4048.5	4058.0	177.0	186.5	9.5	6.19	65.2
C0024G-11X	ESCS	23 Mar 2019 1818	35	4058.0	4067.5	186.5	196.0	9.5	6.74	70.9
C0024G-12X	ESCS	23 Mar 2019 2008	28	4067.5	4077.0	196.0	205.5	9.5	1.80	18.9
C0024G-13X	ESCS	23 Mar 2019 2256	42	4077.0	4077.0	205.5	215.0	9.5	5.30	55.8
C0024G-14X	ESCS	24 Mar 2019 0221	35	4077.0	4086.3	205.5	213.0	9.5 9.5	6.00	63.2
C0024G-14X	ESCS	24 Mar 2019 0412	35	4096.0	4105.5	213.0	234.0	9.5 9.5	7.80	82.1
	ESCS		35 20	4105.5	4105.5	224.5	243.5	9.5 9.5	7.80 9.53	100.3
C0024G-16X		24 Mar 2019 0555								
C0024G-17X	ESCS	24 Mar 2019 0739	22	4115.0	4124.5	243.5	253.0	9.5	3.54	37.3
C0024G-18X	ESCS	24 Mar 2019 1102	26	4124.5	4134.0	253.0	262.5	9.5	4.85	51.1
C0024G-19X	ESCS	24 Mar 2019 1244	18	4134.0	4143.5	262.5	272.0	9.5	7.73	81.4
C0024G-20X	ESCS	24 Mar 2019 1420	20	4143.5	4153.0	272.0	281.5	9.5	5.83	61.4
C0024G-21X	ESCS	24 Mar 2019 1831	23	4153.0	4162.5	281.5	291.0	9.5	3.60	37.9
C0024G-22X	ESCS	24 Mar 2019 2150	27	4162.5	4172.0	291.0	300.5	9.5	7.90	83.2
C0024G-23X	ESCS	24 Mar 2019 2339	23	4172.0	4181.5	300.5	310.0	9.5	5.20	54.7
C0024G-24X	ESCS	25 Mar 2019 0333	26	4181.5	4191.0	310.0	319.5	9.5	8.80	92.6

Table T5. Drilling summary, Site C0025.

				Depth (mbsf)				Core recovery			Date (2019)		
Hole	Latitude	Longitude	Water depth (mbsl)	Тор	Bottom	Cores (N)	Advanced (m)	(m)	(%)	Cored interval (m)	Start	Finish	Days in hole
C0025A	33°24′05.4600″N	136°20′09.1428″E	2039.5	0.0	580.5	19	180.5	123.02	68.2	400.0-580.5	26 Mar	30 Mar	4

Table T6. Summary of operations and significant events, Expedition 358, Sites C0002, C0024, and C0025. (This table is available in CSV format only.)

Table T7. Coring summary, Hole C0025A. RCB = rotary coring barrel.

	Coring system	Time on deck	Coring time	Depth	BRT (m)	Depth	n (mbsf)		Recovery	
Hole, core	(inches)	(h)	(min)	Тор	Bottom	Тор	Bottom	Advanced (m)	(m)	(%)
C0025A-1R	10-5/8 RCB	27 Mar 2019 1103	39	2440	2449	400	410	10	11	115
C0025A-2R	10-5/8 RCB	27 Mar 2019 1335	29	2449	2459	410	419	10	0	0
C0025A-3R	10-5/8 RCB	27 Mar 2019 1625	15	2459	2468	419	429	10	4	37
C0025A-4R	10-5/8 RCB	27 Mar 2019 1946	21	2468	2478	429	438	10	7	75
C0025A-5R	10-5/8 RCB	27 Mar 2019 2228	15	2478	2487	438	448	10	9	98
C0025A-6R	10-5/8 RCB	28 Mar 2019 0101	14	2487	2497	448	457	10	10	102
C0025A-7R	10-5/8 RCB	28 Mar 2019 0333	19	2497	2506	457	467	10	9	96
C0025A-8R	10-5/8 RCB	28 Mar 2019 0551	18	2506	2516	467	476	10	6	62
C0025A-9R	10-5/8 RCB	28 Mar 2019 0802	18	2516	2525	476	486	10	5	50
C0025A-10R	10-5/8 RCB	28 Mar 2019 1025	17	2525	2535	486	495	10	4	46
C0025A-11R	10-5/8 RCB	28 Mar 2019 1252	18	2535	2544	495	505	10	9	90
C0025A-12R	10-5/8 RCB	28 Mar 2019 1531	14	2544	2554	505	514	10	9	96
C0025A-13R	10-5/8 RCB	28 Mar 2019 1811	15	2554	2563	514	524	10	10	103
C0025A-14R	10-5/8 RCB	28 Mar 2019 2025	20	2563	2573	524	533	10	9	93
C0025A-15R	10-5/8 RCB	28 Mar 2019 2252	17	2573	2582	533	543	10	9	93
C0025A-16R	10-5/8 RCB	29 Mar 2019 0124	17	2582	2592	543	552	10	4	37
C0025A-17R	10-5/8 RCB	29 Mar 2019 0346	20	2592	2601	552	562	10	4	37
C0025A-18R	10-5/8 RCB	29 Mar 2019 0820	17	2601	2611	562	571	10	3	28
C0025A-19R	10-5/8 RCB	29 Mar 2019 1058	18	2611	2620	571	581	10	4	39

Figure F1. NanTroSEIZE transect map. Transect lines a and b refer to composite seismic depth section of Figure F2A and Line ODKM-B of Figure F2B, respectively. Solid dots = Expedition 358 sites, open dots = previous NanTroSEIZE sites.

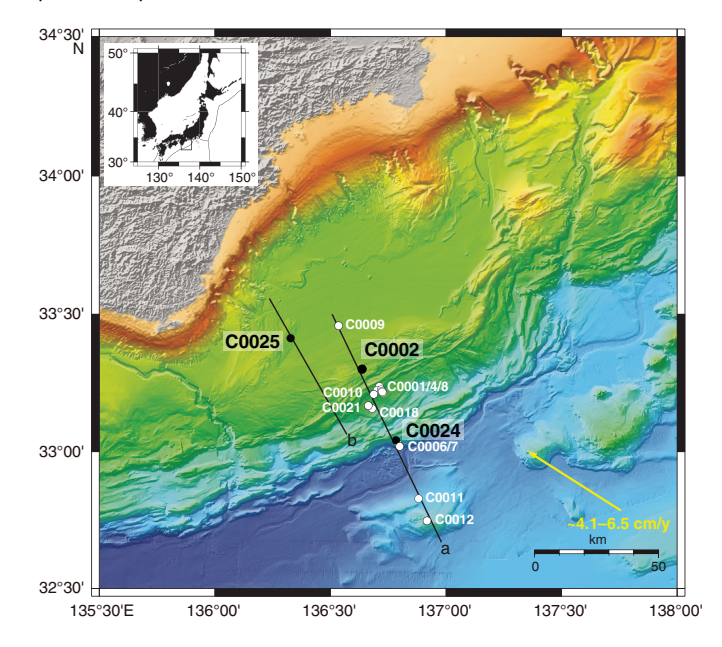


Figure F2. A. Regional seismic reflection depth-processed imaging for Sites C0002 and C0024 and other previously drilled NanTroSEIZE sites. PTZ = protothrust zone. B. Japan Agency for Marine-Earth Science and Technology (JAMSTEC) Seismic Reflection Line ODKM-B with location of Site C0025.

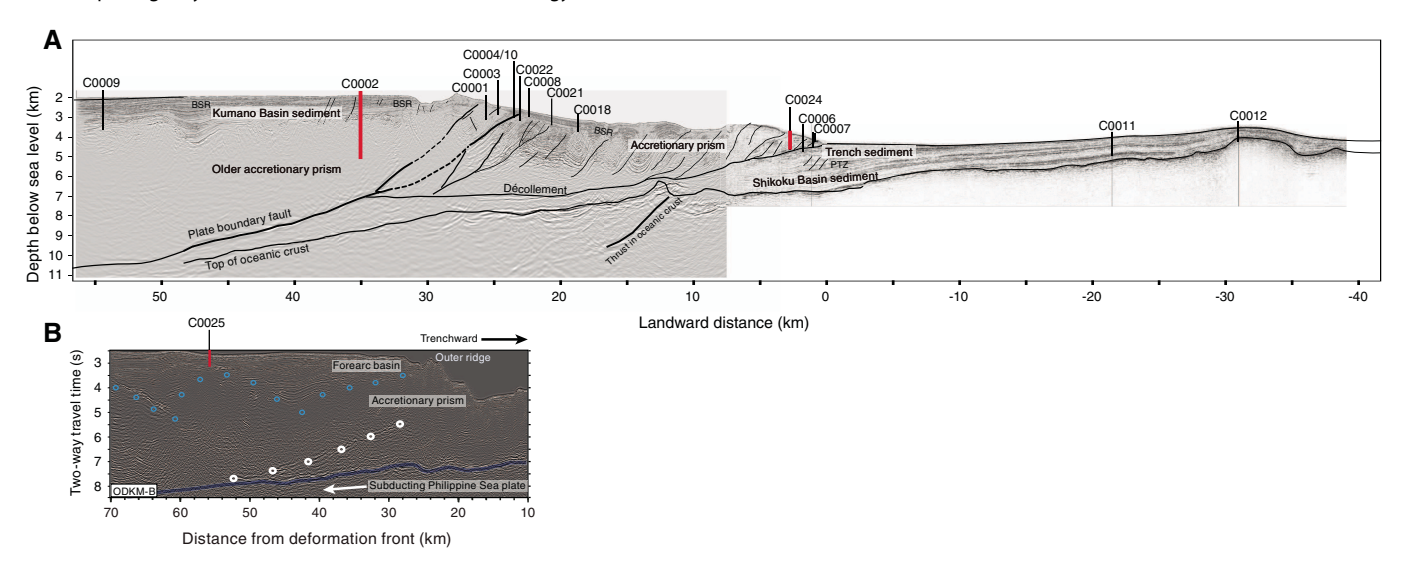


Figure F3. Seismic cross sections near Site C0002. VE = vertical exaggeration. A. In-line (IL). B. Cross-line (XL).

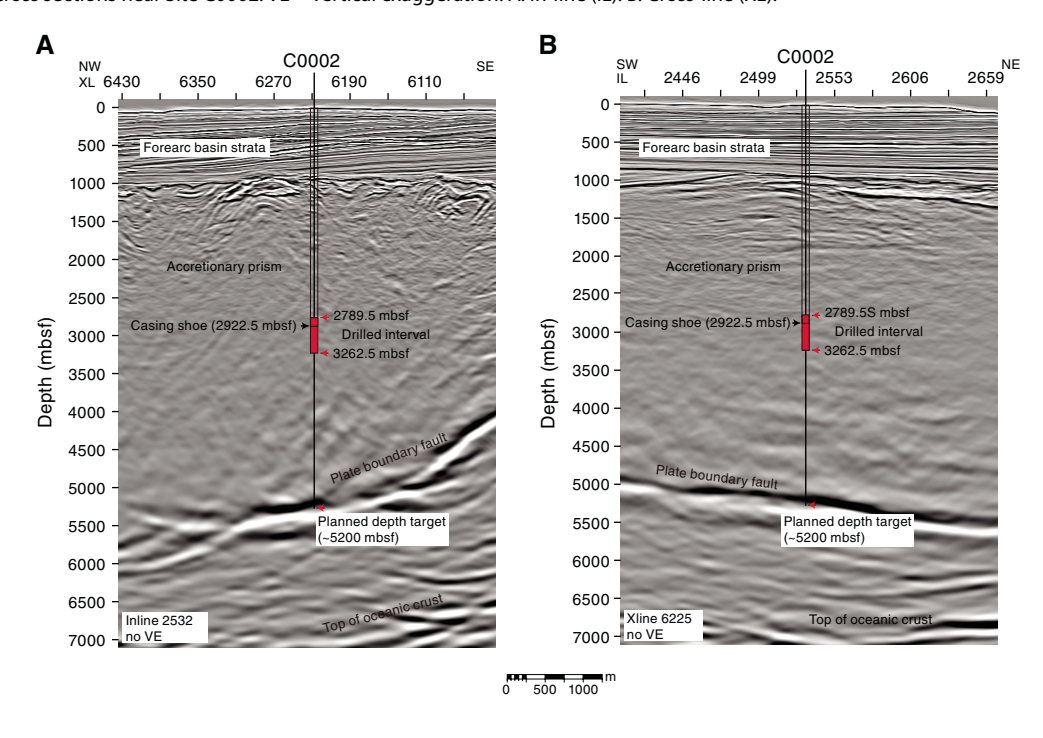


Figure F4. Schematic diagrams (not to scale). A. Holes C0002F/C0002N/C0002P drilled during previous expeditions. WH = wellhead. MSL = from mean sea level. Horizontal black line between blue and white bands = seafloor. B. Expedition 358 drilling and casing plan, building downward from preexisting Hole C0002P. C. Actual holes drilled during Expedition 358. Note the change in relative scale compared to A and B.

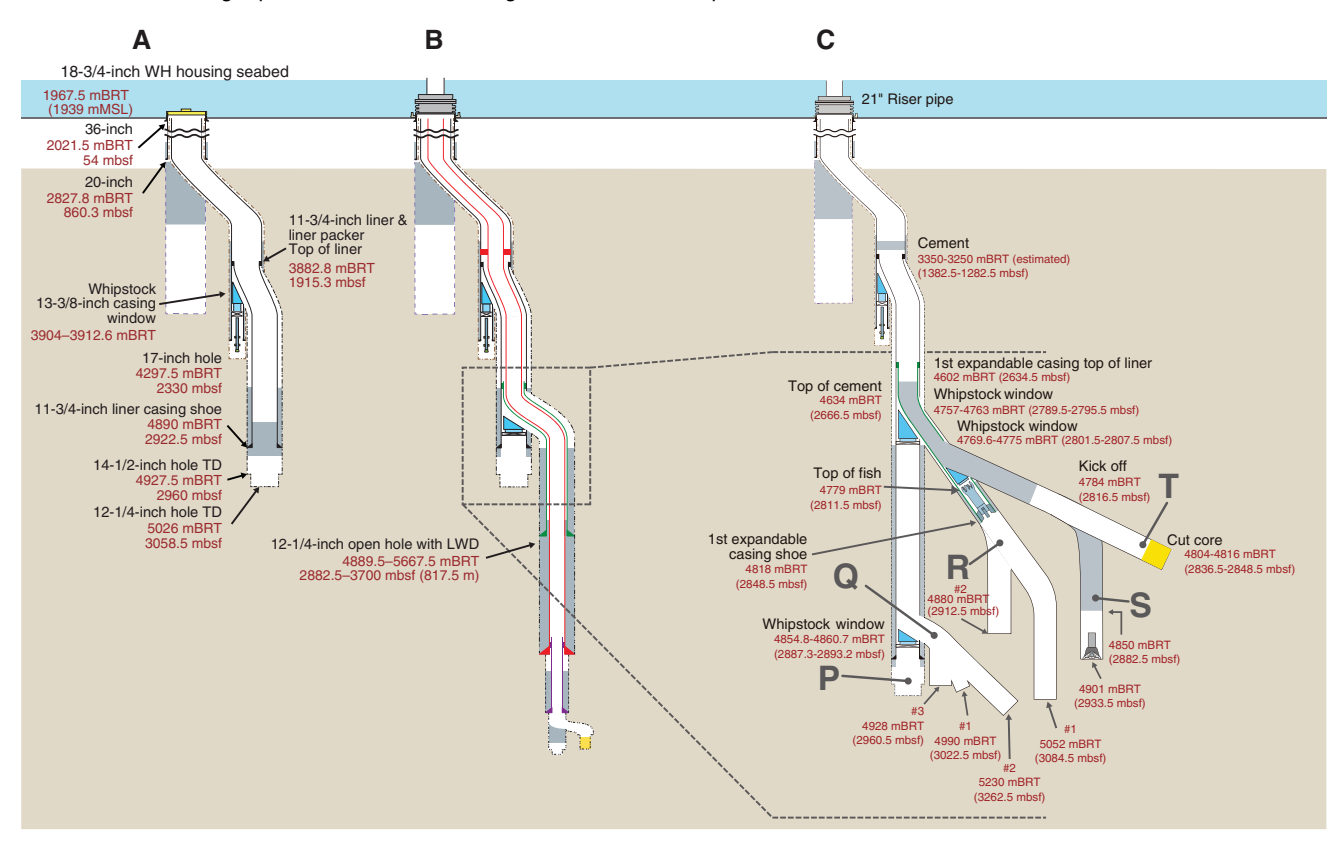


Figure F5. Summary of (A) all holes drilled at Site C0002 from 2007 through 2019 and (B) sidetrack holes and depth ranges drilled at Site C0002 during Expedition 358 (see Figure F4C for their connections to each other and relative geometry). Numbers are specific depths in meters below seafloor of the top and bottom of each sidetrack hole.

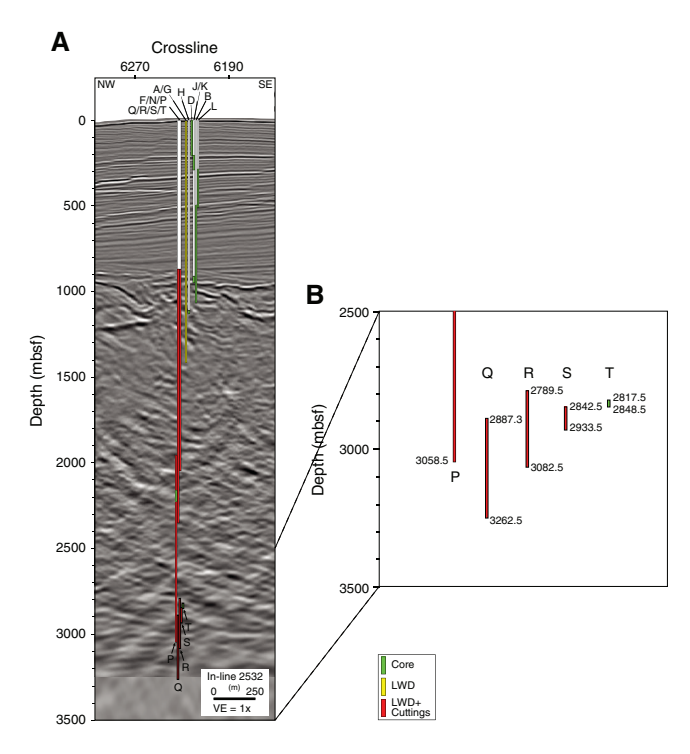


Figure F6. A, B. Summary of results, Site C0002. Proportion of lithology is shown next to the cuttings composite section image. $V_P = P$ -wave velocity, GR = gamma ray. (Continued next page.)

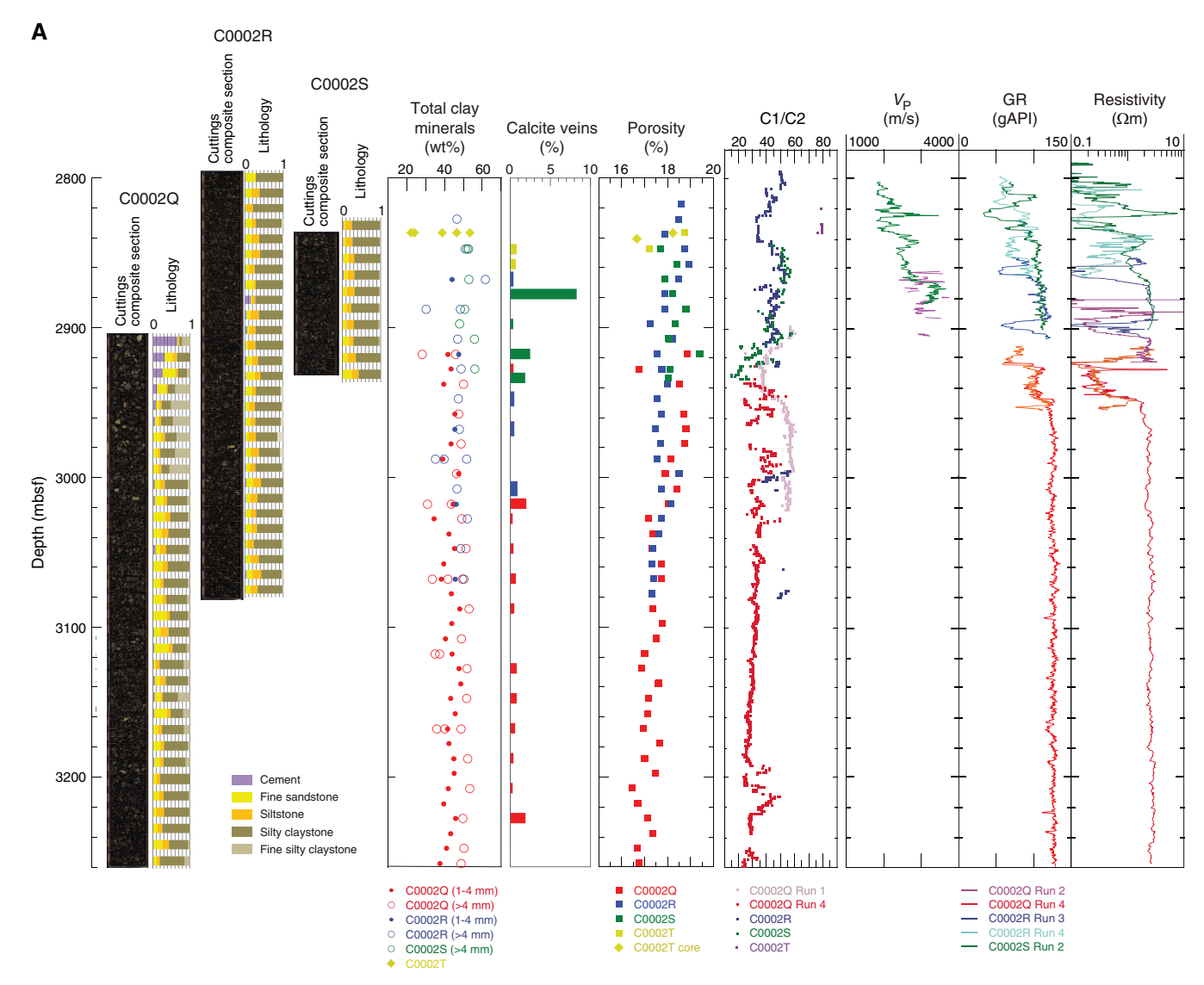


Figure F6 (continued).

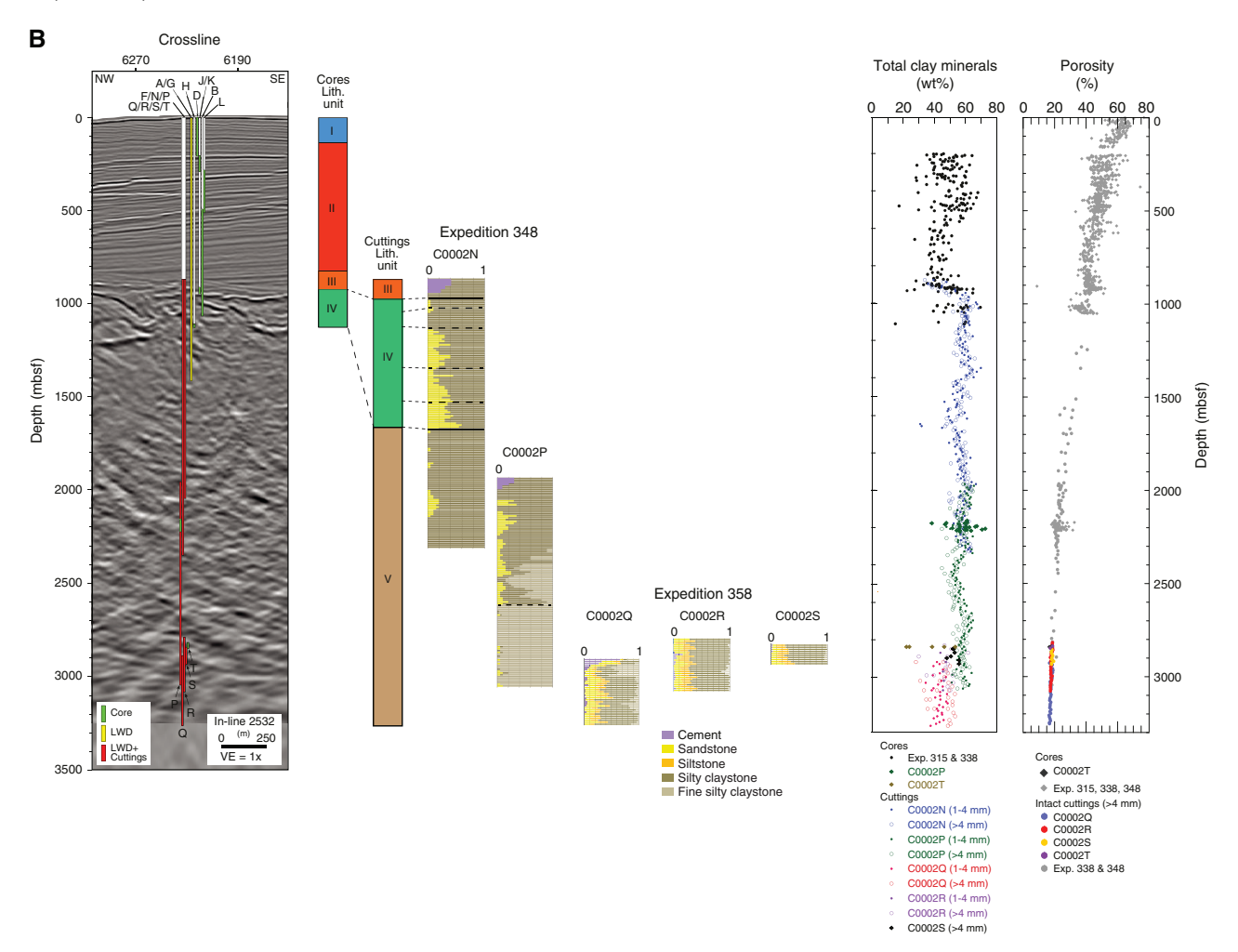


Figure F7. Interpreted seismic depth section of In-line 2437 in the frontal thrust region with locations of Sites C0024, C0006, and C0007. Colored shading = seismic stratigraphic packages, red = faults (bold for major faults), yellow = Site C0024 logging-while-drilling and coring holes.

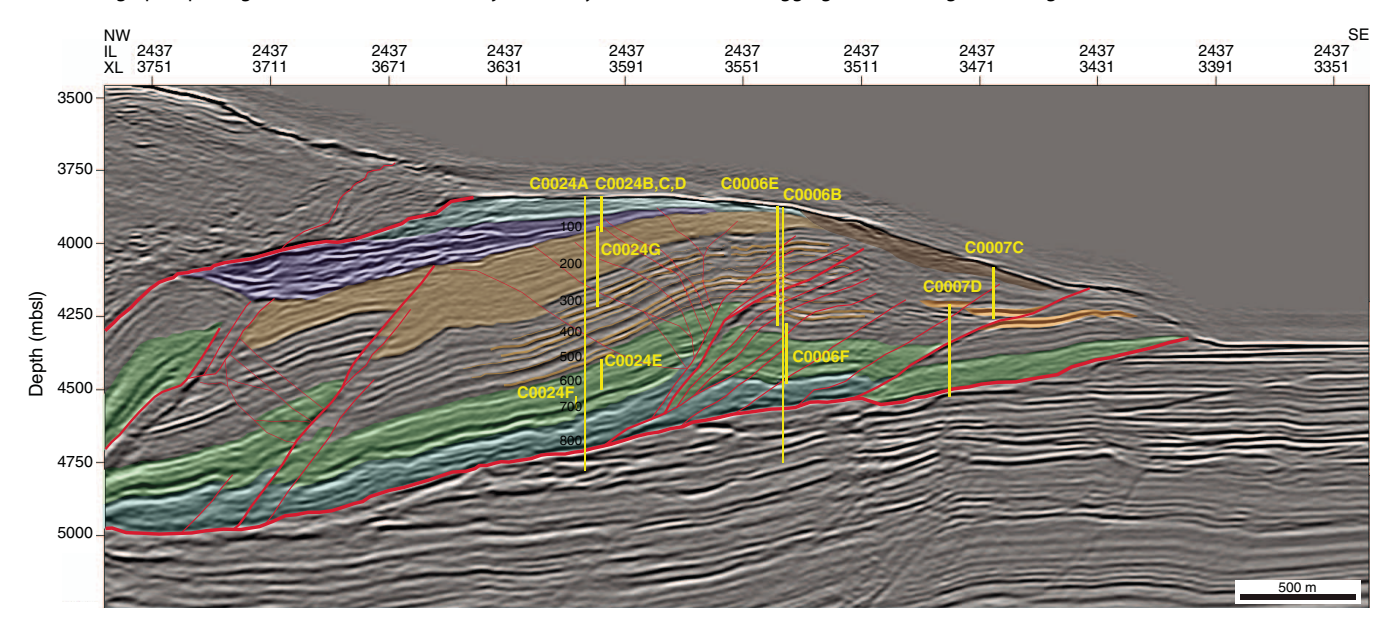


Figure F8. Summary of results, Site C0024. A. Core-based results. (Continued next page.)

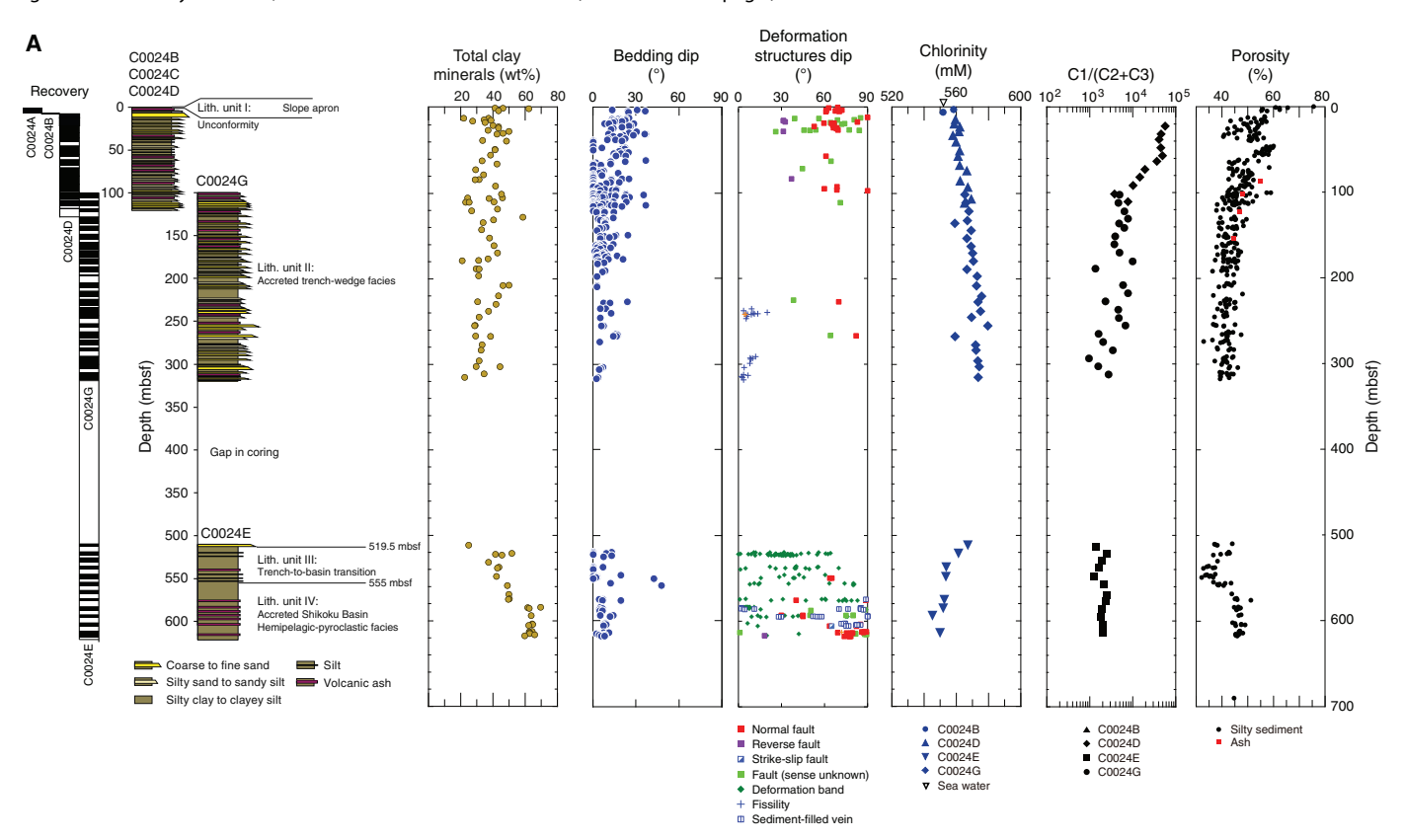


Figure F8 (continued). B. Logging data. RAB = resistivity-at-the-bit tool.

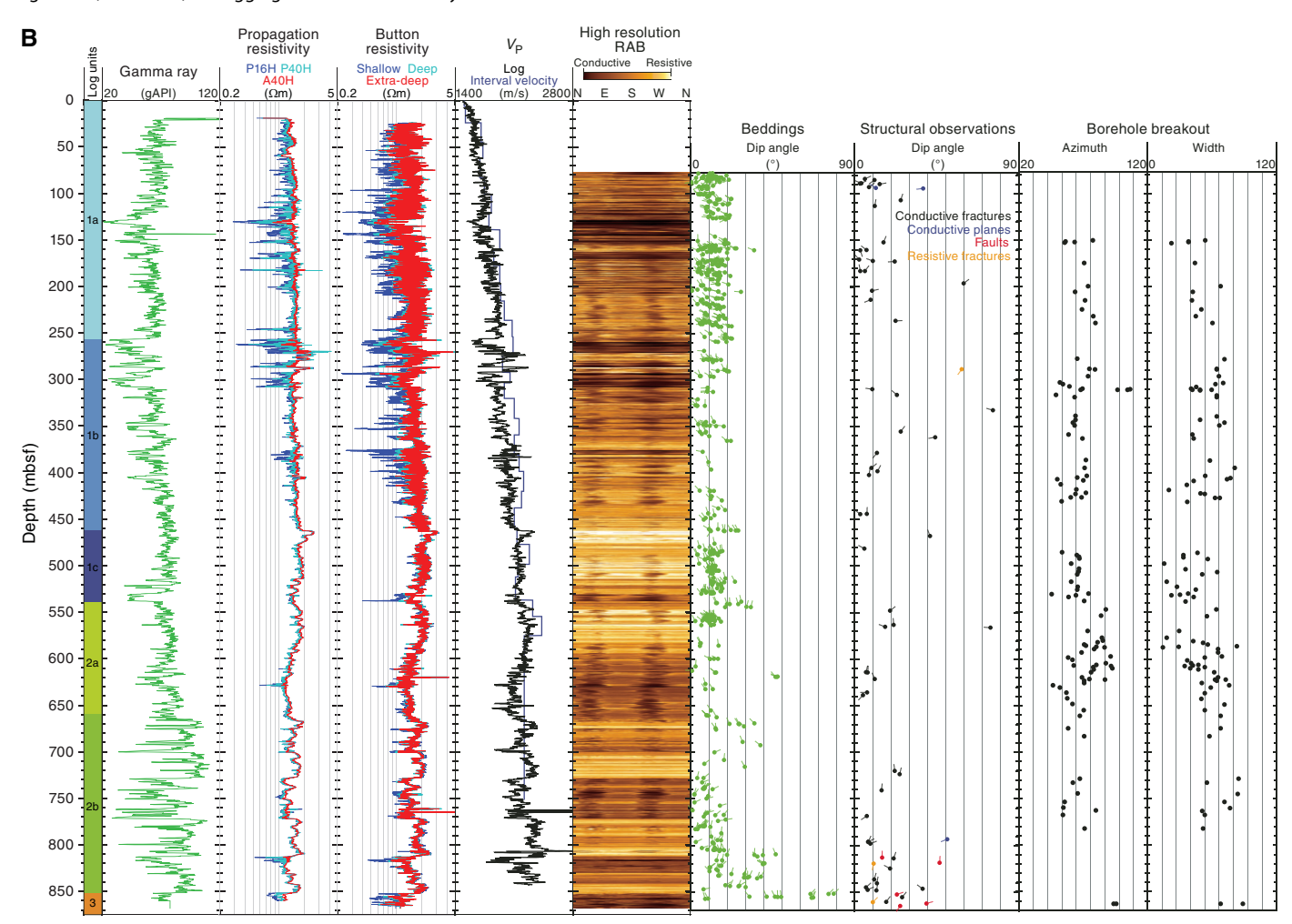


Figure F9. Logging data from plate boundary fault zone, Site C0024. UHRI = ultrahigh-resolution image, Res = resistivity, BIT = bit, BX = extra deep button, BD = deep button, BM = medium button, BS = shallow button.

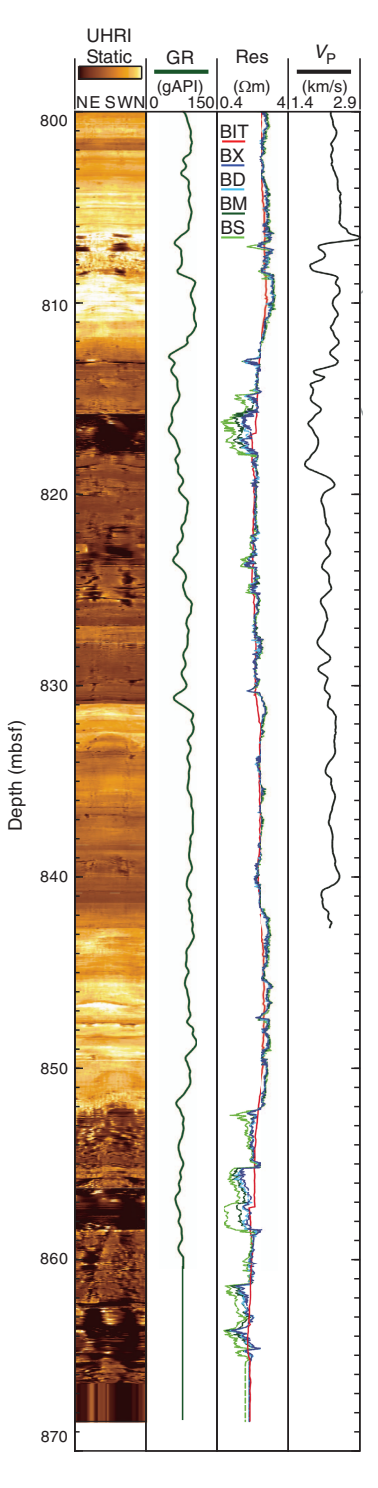


Figure F10. Seismic cross section near Site C0025.

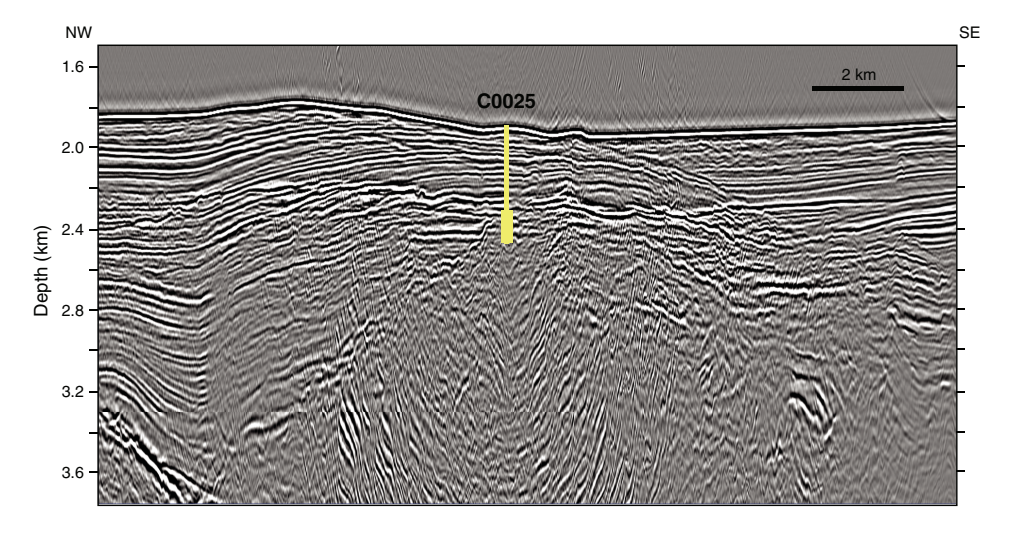


Figure F11. Summary of results, Site C0025. Triangles on chlorinity (blue) and boron (green) plot indicate seawater values.

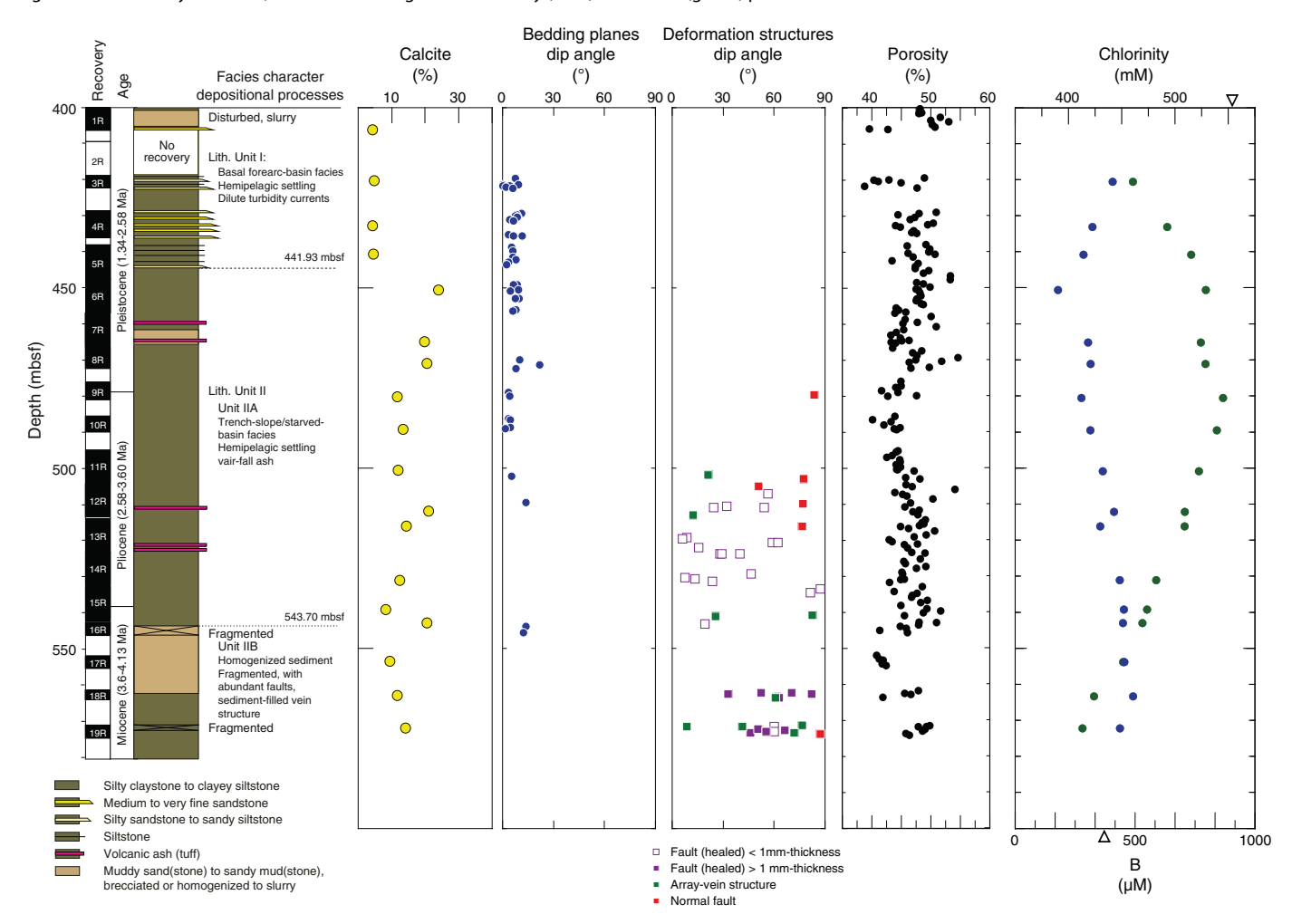


Figure F12. (A) Photo image logger (MSCL-I) and (B) X-ray computed tomography (CT) images parallel to split core surface (358-C0025A-19R-3, 40–64.5 cm) illustrating sediment-filled veins (green arrows), cohesive healed faults (purple arrows), and a normal fault (red arrows). On X-ray CT images, cohesive healed faults are brighter than the surrounding matrix and correspond to higher X-ray CT number and density. The normal fault can be identified because it displaces array vein structures (X-ray CT images). Sediment-filled vein structures are generally resolved on X-ray CT images and occur as bright features filled with higher density material. Thinner sediment-filled vein structures are not resolved (X-ray CT images).



Figure F13. Area map, Site C0024. Open dots = Expedition 314 and 316 sites, black dots = Expedition 358 logging-while-drilling and coring holes, yellow dots = original proposed locations of Site NT1-03C holes.

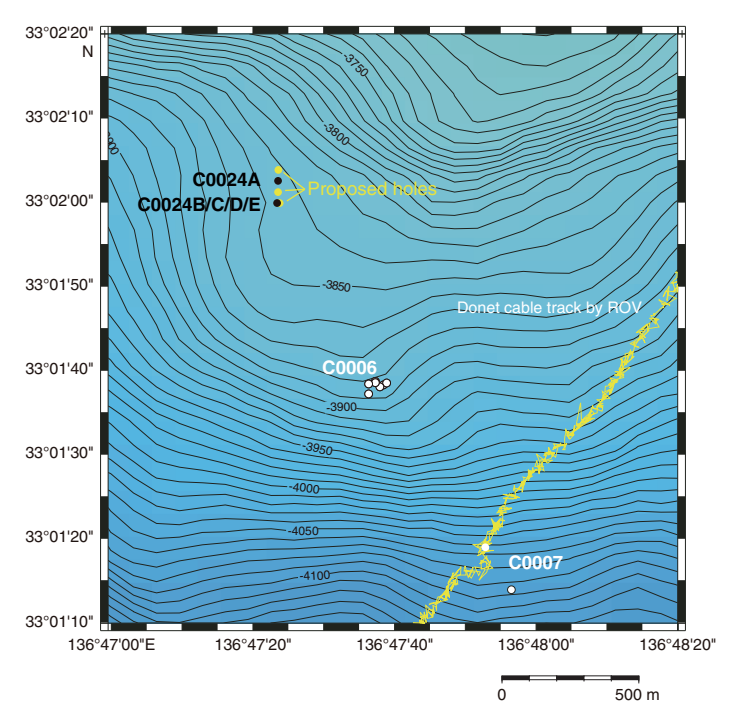


Figure F14. Bathymetric map, Site C0025.

